

Contents lists available at ScienceDirect

Petroleum Science

journal homepage: www.keaipublishing.com/en/journals/petroleum-science



Original Paper

Coupled effects of paleofluid evolution on ultra-deep microbialite reservoir modification: A case study of the upper Ediacaran Deng-2 member within the Penglai area of Central Sichuan Basin, SW China



Xin Jin ^a, Jin-Min Song ^{a, *}, Shu-Gen Liu ^{a, b}, Bin Wang ^a, Di Yang ^a, Zhi-Wu Li ^a, Li-Zhou Tian ^a, Hao-Shuang Deng ^a, Shan Ren ^a, Jia-Min Xue ^a, Jia-Xin Guo ^a, Zhao-Yi Zhang ^a, Xing-Peng Shao ^a

ARTICLE INFO

Article history: Received 1 April 2024 Received in revised form 1 July 2024 Accepted 8 October 2024 Available online 11 October 2024

Edited by Jie Hao

Keywords:
The Deng-2 member
Paleofluid evolution
Ultra-deep microbialite reservoirs
Ediacaran
Sichuan basin

ABSTRACT

Paleofluid-rock interaction results in the modification of the ultra-deep reservoir quality, but the coupling effects of the paleofluid evolution on reservoir quality modification are still underestimated. Here, the multi-stage dolomite cements have been studied by means of core observations, thin section identification, fluid inclusions, and in situ elements and isotopic analyses in order to reaveal the paleofluid evolution processes and their effects on the reservoir quality. The fibrous dolomite cement (FDC) and bladed dolomite cement (BDC) both have similar geochemical properties and homogenization temperature (Th) to the matrix dolostone. Subsequent early silicification occurs (QZ1). However, silt-to fine-sized crystalline dolomite cement (CD2) has higher concentration of Fe and medium rare earth element, more negative δ^{18} O than for FDC and BDC, and 103.4–150.2 °C in Th. The first petroleum charge episode solid bitumen 1 (SB1) followed the CD2. The medium to coarse sized crystalline dolomite cement (CD3) is characterized by the higher Mn and lower Sr concentration than CD2, positive δEu anomaly, negative δ^{13} C and δ^{18} O, high δ^{87} Sr δ^{86} Sr ratio and 138.9 °C—184.3 °C in Th. The solid bitumen 2 (SB2) occurs after CD3. Subsequently, the saddle dolomite (SD) has higher Fe and Mn concentration and lower Na and Sr than others cement, δ Eu positive anomaly, negative δ^{13} C and δ^{18} O, high 87 Sr/ 86 Sr ratio and 177.5 °C -243.6 °C in Th. Eventually massive silicification (QZ2) took place. The FDC, BDC, QZ1 and SB1 formed in the early diagenetic stage and have little negative effect on the reservoir quality. But the CD2 and CD3 dramatically decreased the reservoir quality related to a quantity of hydrothermal fluids entrance in the mesodiagenetic stage along the strike-slip faults and the unconformity surface at top of the Deng-2 Member during the late stage of the Caledonian orogeny. The reservoir spaces were retained and enlarged during the late diagenetic stage when the peak petroleum charge occurred, massive silicification and thermochemical sulfate reduction took place with SB2, SD and QZ2 being formed. The research outcome may update our understanding on the retention mechanism and the insights for further hydrocarbon exploration of Precambrian ultra-deep microbial reservoirs.

© 2024 The Authors. Publishing services by Elsevier B.V. on behalf of KeAi Communications Co. Ltd. This is an open access article under the CC BY-NC-ND license (http://creativecommons.org/licenses/by-nc-nd/4.0/).

1. Introduction

The hydrocarbon exploration activities have been entering the ultra-deep (>6000 m) carbonate reservoirs in China as well as

* Corresponding author.

E-mail address: songjinmin2012@cdut.edu.cn (J.-M. Song).

elsewhere in the world recently (Fainstein et al., 2019; Cruz et al., 2021; Da Cruz et al., 2021; He et al., 2021; Hu et al., 2020a, 2023), which promotes the discussion of the ultra-deep reservoir porosity destruction and preservation. It is normally thought that the reservoir porosity has been cemented during the burial process (Ehrenberg et al., 2009; Meng et al., 2024), but the fact that high-quality pores and vugs have been preserved under ultra-deep burial conditions has refresh our understanding on the reservoir

a State Key Laboratory of Oil and Gas Reservoir Geology and Exploitation, Chengdu University of Technology, Chengdu, 610059, Sichuan, China

^b Xihua University, Chengdu, 610039, Sichuan, China

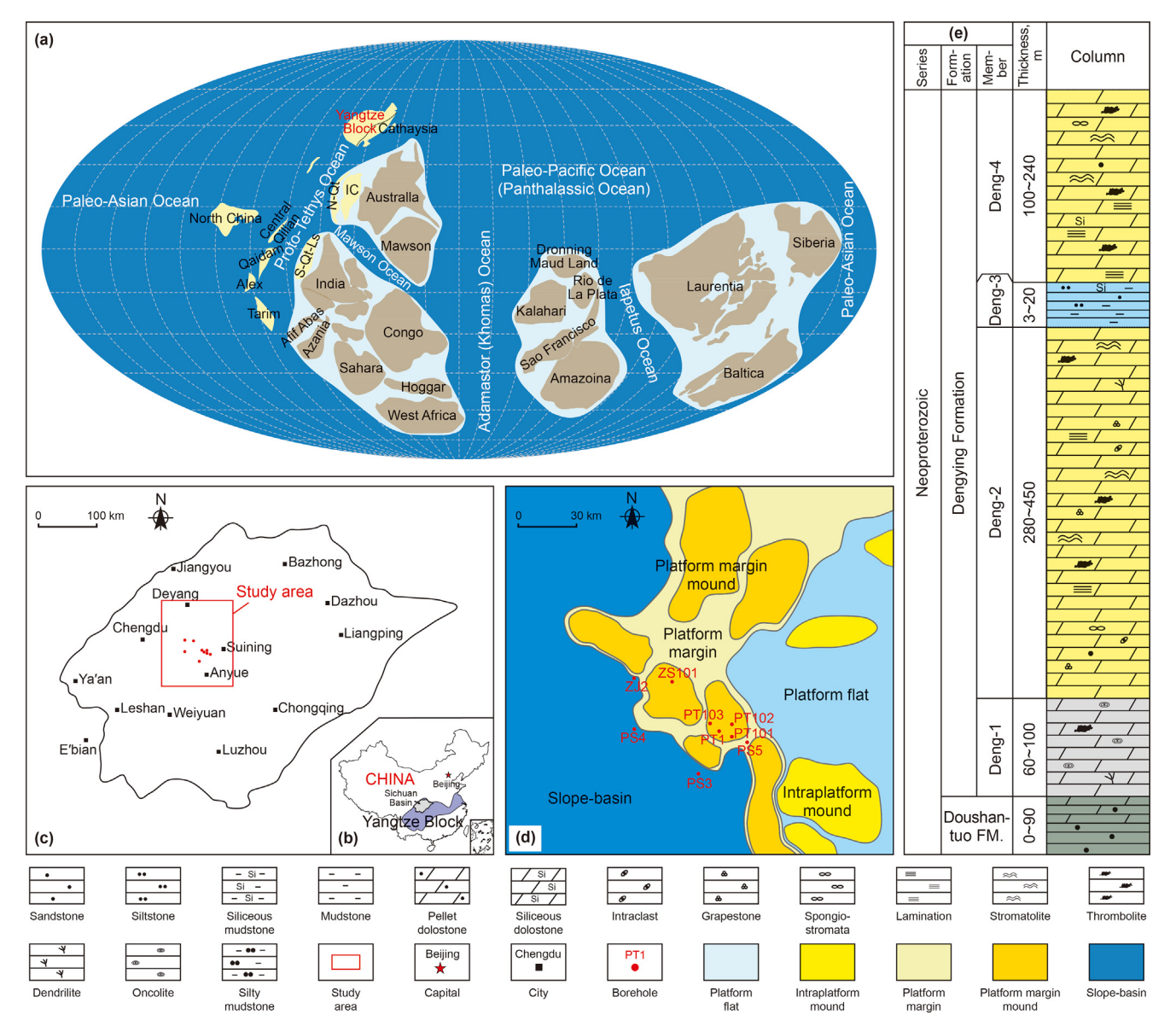


Fig. 1. (a) Distribution of continental blocks during the Upper Neoproterozoic (Zhao et al., 2018); (b) Location map of the Yangtze Plate; (c) Structural elements of the Sichuan Basin; (d) Sedimentary facies of the Deng-2 Member in the Penglai Area (Fan et al., 2022); (e) Representative stratigraphic column of the Dengying Formation.

geology (Su et al., 2021; Wang et al., 2023a,b,c). Tectonic and sedimentary control carbonate mineral composition, texture type and primitive pore development (He et al., 2017), which are the material basis for the development of ultra-deep carbonate reservoirs, whereas epigenetic karst (Hu et al., 2020b; Zhao et al., 2021), hydrothermal effects (Xu et al., 2022; Li et al., 2023), thermal sulfate reduction (TSR) (Cai et al., 2014; Jiang et al., 2018a,b; Zhu et al., 2020; Li et al., 2024), deep-buried hydrocarbon production and conversion (He et al., 2017), and other fluid evolution (Zhao et al., 2012; He et al., 2017; Ma et al., 2023) control the further development and maintenance of the reservoirs, so that the reservoir space is adjusted. This implies that reconstruction of fluid circulation events and reservoir diagenetic history is a prerequisite for understanding reservoir pore evolution (James et al., 2009; Zhou et al., 2020). Cement and fluid inclusions are rich in geological information and are widely used to track the geological fluid transport and formation history of reservoirs (Bourdet et al., 2010; Dai et al., 2018; Huang et al., 2021). However, it remains a large challenge to

quantitatively evaluate the coupled effect of every-stage of paleofluid evolution and ultra-deep carbonate reservoir modification nowadays.

The Ediacaran Dengying Formation microbialite reservoirs have considerable complexity and heterogeneity, as a result of the multiple tectonic phase and paleofluid activities. Although it is widely accepted that microbiome composition, karst action, and subsequent hydrothermal action determine reservoir configuration and distribution (Zou et al., 2014; Jiang et al., 2016; Feng et al., 2017; Song et al., 2018; Zhou et al., 2020; Yan et al., 2022). However, the fact that fluid evolution processes and their connection to the pore system have not been thoroughly investigated has led to a persistent underestimation of the relative proportions of fluid contributions to reservoir destruction and preservation during the diagenetic process. The microbialite reservoirs of the upper Ediacaran Deng-2 Member within the Penglai area have been the subject of recent exploration for natural gas in the burial depth of 5700 m—6300 m, which provides a suitable case study for the

quantitative evaluation of the coupled effect of paleofluids evolution on ultra-deep microbial carbonate reservoir modification based on core descriptions, thin section identification, fluid inclusions, and geochemical analyses such as C-O-Sr isotopes, major elements and trace elements analysis within the bulk and *in situ* microzone samples, in order to reveal the multi-phase cementation of the dolomite, determine the origin of the parent fluids, traced the complex fluid evolution history of the Deng-2 Member, and reveal the properties, products and mechanisms of the paleofluid-rock interactions and give insights to the worldwide hydrocarbon exploration on ultra-deep reservoirs.

2. Geological setting

The Sichuan Basin is a typical petroliferous superimposed basin (Liu et al., 2021), located along the western margin of the Yangtze Block. The area was a marine platform from the Ediacaran to the Early Triassic, followed by a terrestrial basin from the Middle Triassic to Eocene, and finally folding, uplift and reworking have occurred since the Oligocene (Liu et al., 2013) (Fig. 1c). The Penglai area is located in the northern Central Sichuan ancient uplift, with an overall north-dipping large-scale monoclinal tectonics, and is

adjacent to the Mianyang-Changning intracratonic sag trough to the west (Yang et al., 2022). The Penglai area has experienced multiple phases of tectonic movements, and two depositional discontinuities existed during the Caledonian and Indochinese phases (Ma et al., 2022). At the end of the depositional period of the Dengving Formation, under the influence of the Tongwan Movement, significant uplift occurred north of Moxi area, and with the continued influence of the Caledonian Movement, it resulted in the partial absence of Ordovician and Cambrian strata in the Penglai area. In the late Hercynian period, the Upper Yangtze Block experienced intracratonic extensional faulting, and the Penglai area began to sink and form a monocline structure. From the late Indosinian period to the present, the low amplitude slope structure was ultimately formed due to the influence of the Longmen Mountain thrust and nappe tectonic movement in western Sichuan Basin (Fan et al., 2022; Shen et al., 2021).

Rift valleys have emerged along the Yangtze Block margin in different directions, such as Kangdian valley in west, Qinling valley in north and Nanhua valley in southeast when it drifted away from the Rodinia supercontinent in the Neoproterozoic era (Fig. 1a and b) (Song et al., 2018; Zhao et al., 2018). The tectonic break-up of Rodinia has also been known as the Xingkai taphrogenesis, which

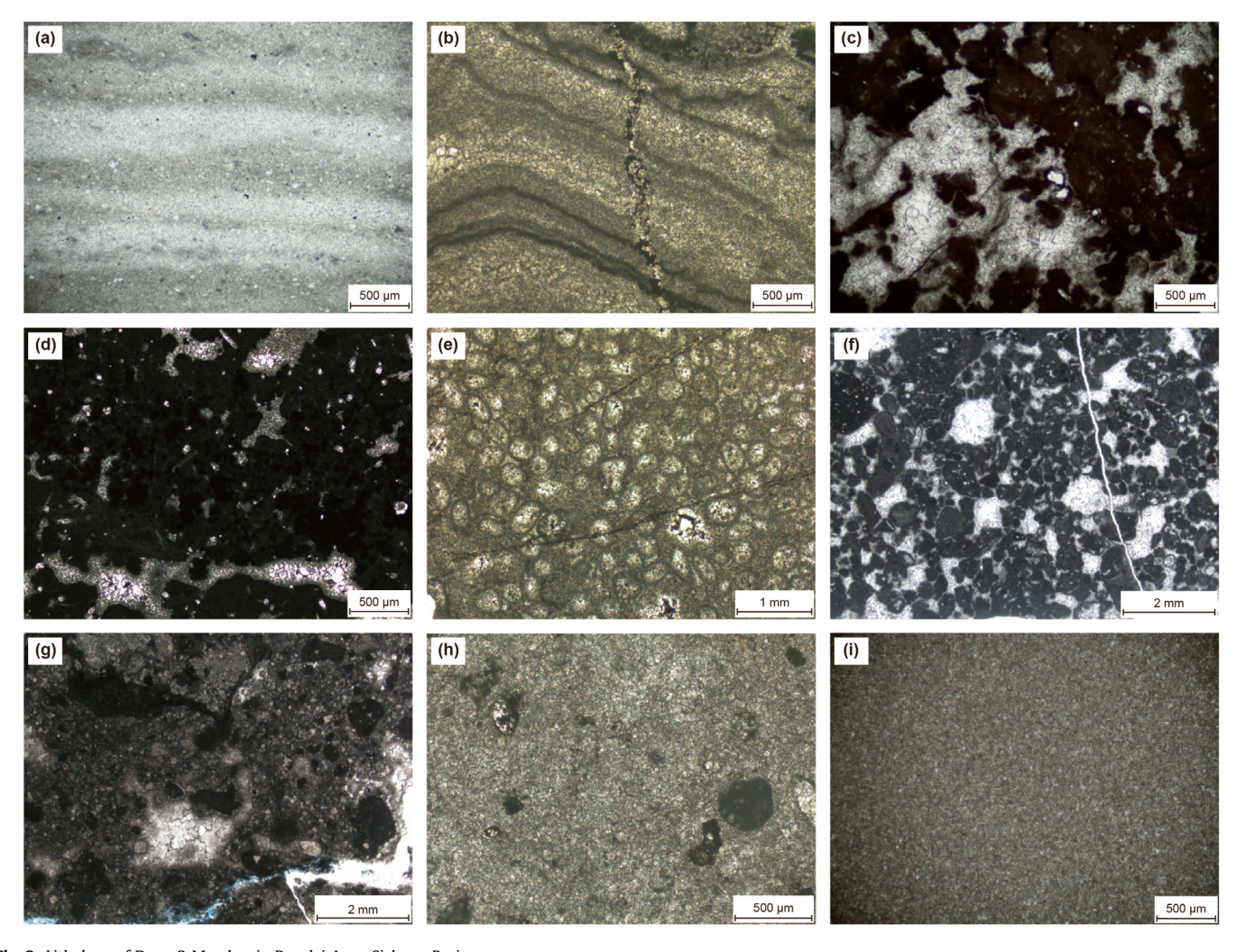


Fig. 2. Lithology of Deng-2 Member in Penglai Area, Sichuan Basin. **(a)** PS4 well, 6230.92m, Stromatolites, × 5, PPL; **(b)** ZJ2 well, 6554.3m, Stromatolites, × 5, PPL; **(c)** PS4 well, 6236.2m, Thrombolites, × 5, PPL; **(d)** PT1 well, 5764.66m, Thrombolites, × 5, PPL; **(e)** PS4 well, 6394.76m, Spongiostromata dolostone, × 2.5, PPL; **(f)** PT101 well, 5711m, Spongiostromata dolostone, × 1.25, PPL; **(g)** PT101 well, 5718.62m, Intraclastic dolopackstone, × 1.25, PPL; **(h)** PS5 well, 5543.58m, Peloidal dolowackestone, × 5, PPL; **(i)** PS4 well, 6234.45m, dolo-mudstone, × 5, PPL: plane-polarized light.

results in the Mianyang-Changning intracratonic sag along the western margin of Sichuan Basin (Liu et al., 2013; Zhong et al., 2013).

The global climate changed from icehouse in the Nanhua period to greenhouse in the Ediacaran. There was a siliciclastic shelf in the Doushantuo Formation and a marine carbonate platform in overlying Dengying Formation (Yu et al., 2011). The shallow water restricted platform dominates in the Dengying Formation, in which

the microbial mound-bank complex and lagoons developed (Fig. 1d). Based on microbe concentration, textures and lithology, the Dengying Formation has been subdivided into the Deng-1 (base), Deng-2, Deng-3 and Deng-4 (top) Members (Zhai et al., 2020) (Fig. 1c). The Deng-1 Member is characterized by dolomudstone and laminated dolostone. The Deng-2 Member consists mostly of botryoidal dolostone and thrombolitic dolostone. At the top of the Deng-2 is a regional unconformity that separates Deng-2

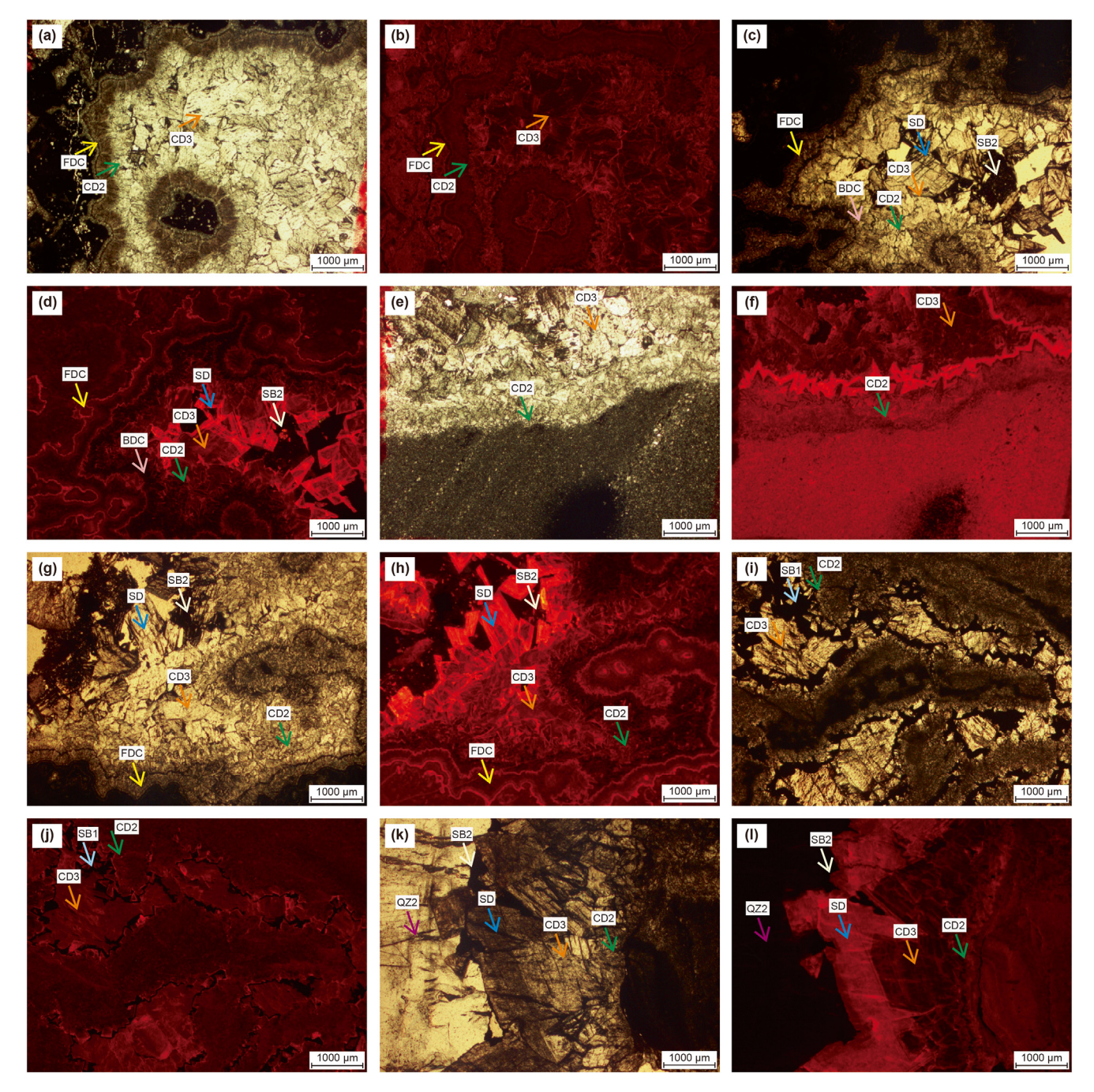


Fig. 3. Cementation in the Deng-2 Member, Penglai Area, Sichuan Basin.
(a) PT1 well, 5771.3 m, Thrombolites, FDC (yellow arrow), CD2 (green arrow), CD3 (orange arrow), × 2.5, PPL; (b) CL of Fig. 3(a); (c) PT102 well, 5840.67 m, Thrombolites, FDC (yellow arrow), BDC (pink arrow), CD2 (green arrow), CD3 (orange arrow), SD (bule arrow), SB2 (white arrow), × 2.5, PPL; (d) CL of Fig. 3(c); (e) PT1 well, 5766.62 m, dolo-mudstone, CD2 (green arrow), CD3 (orange arrow), × 2.5, PPL; (f) CL of Fig. 3(e); (g) PT102 well, 5840.85 m, Thrombolites, FDC (yellow arrow), CD3 (orange arrow), CD3 (orange arrow), SD (bule arrow), SB2 (white arrow), × 2.5, PPL; (f) CL of Fig. 3(g); (i) PT102 well, 5870.75 m, dolo-mudstone, CD2 (green arrow), SB1 (light blue arrow), CD3 (orange arrow), × 2.5, PPL; (j) CL of Fig. 3(i); (k) PT102 well, 5872.14 m, Thrombolites, CD2 (green arrow), Bit2 (light blue arrow), CD3 (orange arrow), SD (bule arrow), SB2 (white arrow), CD3 (purple arrow

and Deng-3 Members (Fig. 1e). The Deng-3 Member is comprised of mudstone, argillaceous siltstone interbedded with dolomudstone and tuff. The Deng-4 Member is composed of laminations, stromatolites, and silica dolostone (Liu et al., 2016b; Song et al., 2017). At the top of Deng-4 Member, there is a regional unconformity that separates the Ediacaran and Lower Cambrian (Zhao et al., 2022).

3. Sampling and methods

A total of 127 samples were collected from Deng-2 Member at

five wells in the Penglai area. In order to study the palaeofluid evolution, we focused on sampling for half-filled pores and fractures, and fully filled pores and fractures. Thin sections were made for the samples and petrographic analysis was performed using an Olympus BX60 microscope. Based on the thin section observations, samples were selected for further geochemical analyses. Powders were extracted from 17 matrix samples and 20 cement using microdrilling methods for major and trace elements analysis and Whole-rock C-O-Sr isotopes analyses. Up to 53 points of *in situ* trace element analysis were carried out on different cementation stages

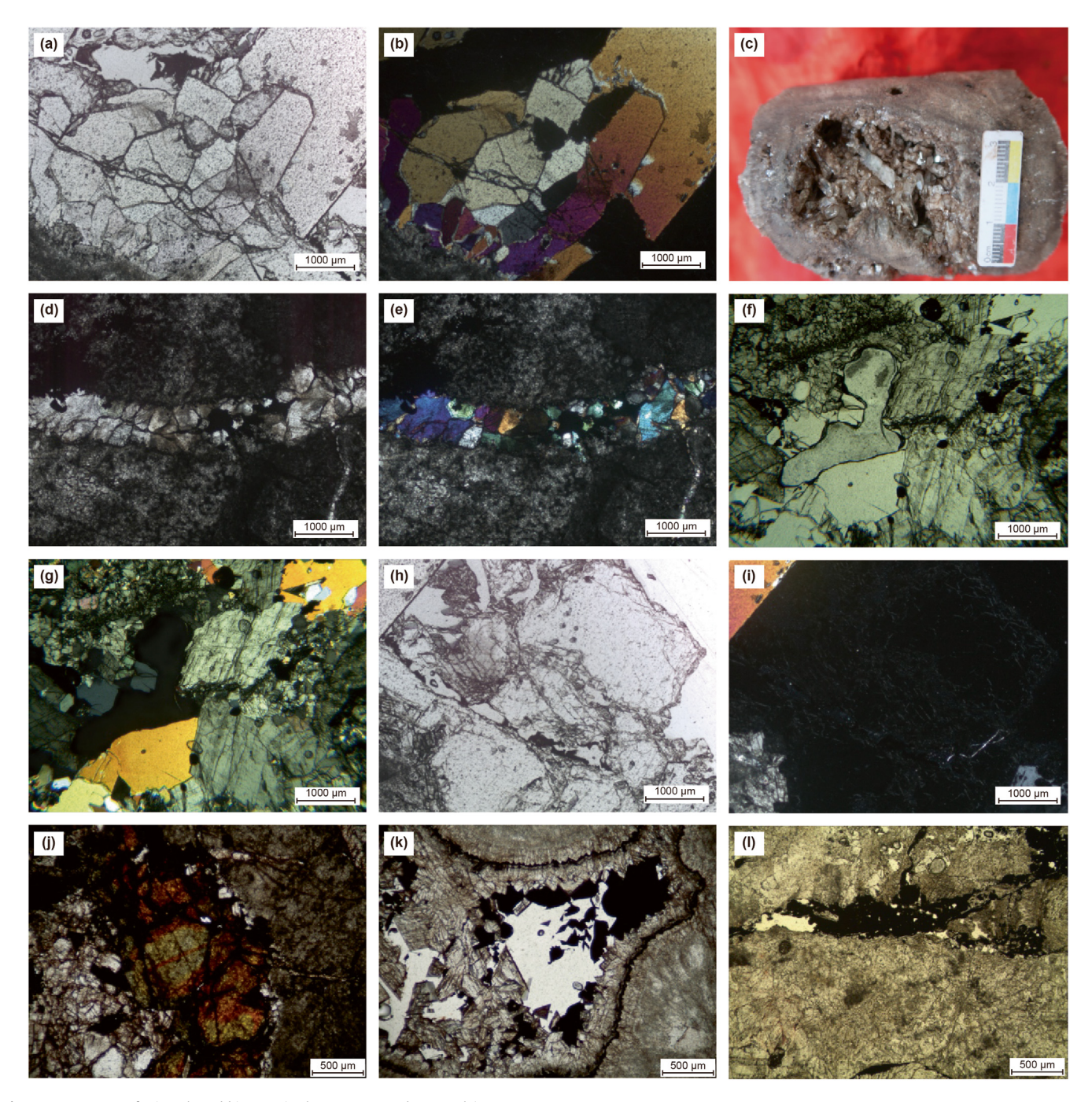


Fig. 4. Occurrences of minerals and bitumen in the Deng-2 Member, Penglai area.

(a) PT102 well, 5875.65 m, QZ1, selective silicification, × 2.5, PPL; (b) CPL of (a); (c) PT102 well, 5882.09 m, QZ2; (d) PT102 well, 5879.50 m, QZ2, siliceous vein, non-selective silicification, × 2.5, PPL; (e) CPL of (d); (f) PT1 well, 5789.72 m, QZ2, non-selective silicification, × 2.5, PPL; (g) CPL of (f); (h) PT102 well, 5875.65 m, fluorite, × 2.5, PPL; (i) CPL of (h); (j) PS4 well, 6223.66 m, sphalerite, × 5, PPL; (k) PS4 well, 6231.96 m, Two phase bitumen filling, × 5, PPL; (l) PT1 well, 5778.84 m, SB2, × 5, PPL PPL: plane-polarized light, CPL: cross polarized light.

of 10 samples to obtain their major and minor element abundances. Up to 50 points of $in\ situ$ laser carbon and oxygen isotope analysis were carried out on different cements of 8 samples. 40 samples were cut into 100 μ m thick slices for observation and measurement of fluid inclusions in the different cements, yielding 223 groups homogenization temperatures (Th) and ice temperatures (Tm).

The major and trace elements analysis was completed at the Research Institute of Qinghai-Tibetan Plateau, Chinese Academy of Sciences. The major element analysis was conducted using an Inductively Coupled Plasma Optical Emission Spectrometer (ICP-OES), and the data are reported in ppm. Trace element analysis was conducted using an Inductively Coupled Plasma Mass Spectrometer ELAN DRC-e ICP-MS, and the results are reported in ppm.

Whole-rock carbon and oxygen isotope analyses were completed at the National Key Laboratory of Oil and Gas Reservoir Geology and Exploitation, Chengdu University of Technology (CDUT). The carbon and oxygen isotopes of carbon dioxide were analyzed using the NBS-18 standardized Finnigan MAT253 mass spectrometer. *In situ* laser carbon and oxygen isotope analysis was completed at PetroChina Hangzhou Research Institute of Geology using a Finnigan MAT253 mass spectrometer. All carbon and oxygen isotope data are reported in % units, relative to the Vienna Pee Dee Belemnite (VPDB) standard. The testing accuracy is higher than $\pm 0.1 \%$.

Strontium isotope analysis was completed at the National Key Laboratory of Oil and Gas Reservoir Geology and Exploitation (CDUT). Strontium isotope analysis was performed using Finnigan MAT-262 thermal ionization mass spectrometer (TIMS).

In situ trace element analysis was completed by Wuhan Sample Solution Analytical Technology Co., Ltd., China. The *in situ* analysis of the trace elements in minerals were determined using the LA-ICP-MS electron probe method. The international standards NIST SRM610 and NIST SRM612 were used for multiple external and internal standard calibration, and the ICPMSDataCal software was used for offline data processing.

The temperature measurement analysis of fluid inclusions was completed at the National Key Laboratory of Oil and Gas Reservoir Geology and Exploitation (CDUT). The Th and Tm of fluid inclusions were measured using the linkam-TH600 polarizing microscope and cooling-heating stage. Salinity was determined based on the Tm values and is reported as wt% NaCl equivalent using the equation wt % NaCl = $1.78 \times \text{Tm} - 0.0442 \times \text{Tm}^2 + 0.000557 \times \text{Tm}^3$ (Bodnar, 1993).

Rare-earth elements (REE) have been standardized by the Post Archean Australian Shale (PAAS) (McLennan, 1989). Eu anomalies (Eu/Eu*), Ce anomalies (Ce/Ce*) and Gd anomalies (Gd/Gd*) are calculated as follow: Eu/Eu* = $2 \times \text{Eu}_n/(\text{Sm}_n + \text{Gd}_n)$ (Bau and Dulski, 1996), Ce/Ce* = Ce_n/($2 \times \text{Pr}_n - \text{Nd}_n$) (McLennan, 1989) and Gd/Gd* = Gd_n/($0.33 \times \text{Sm}_n + 0.67 \times \text{Tb}_n$) (Kulaksız and Bau, 2007), respectively (the sub scripted n means PAAS - normalized).

4. Results

4.1. Petrology textures and cement

4.1.1. Petrology textures

Stromatolite, thrombolite, spongiostromata dolostone, dolopackstone, dolograinstone, dolowackestone and mudstone facies have been observed in the Deng-2 Member of Penglai area through detailed core description and thin section analysis.

The stromatolites are mostly composed of coupled dark and light-colored laminations, which occur in the stromatolitic microbial mat in a layered, columnar or dome shape. The stromatolites usually form cone-shaped structures in macroscopic scale and show characteristic undulate or wavy alternating dark and light

laminations of ~ millimeter thickness under the microscope (Fig. 2a and b).

The thrombolites are composed of irregular patches of mesoscopic and microscopic scale with dolomite cementing fenestral pores (Fig. 2c). The thrombolites are directly related to the Gloeorrh microbial species, which occurs in irregular, dispersed, closely packed or grading into massive micritic clots in shape with dolosparite in coelom and fibrous dolomite rimming vugs.

The spongiostromata dolostone is deposited by the Tortofimria microbial community. It can occur in bubble-like shapes with micritic walls and a dolosparite hollow cavity, with rounded, oval or even polygonal chambered textures (Fig. 2d).

Dolopackstone and dolograinstone occur in thick to massive layers with grain-supported textures that are mostly composed of well-sorted, subrounded to rounded intraclasts. The neomorphic textures and original depositional fabrics such as lamination, thrombolite and oncolite have been observed within the intraclastis in size of 0.5–1.5 mm (Fig. 2e and f).

Dolowackestone and mudstone are mud-supported and thin-to medium-bedded. The dolowackestone usually contain grains in volume of less than 10 %, which are mostly peloidal, with diameters of 0.06 mm—0.1 mm (Fig. 2g and h) with rounded to subrounded shapes and textureless interiors.

4.1.2. Cement characteristics

The fibrous dolomite cement (FDC) and bladed dolomite cement (BDC) both grow along the long axis of crystal. The FDC are mostly composed of dark crystals of 0.03–0.06 mm in diameter. They have a fibrous isopachous lining in the pores and exhibit a dull red color under cathodoluminescence (CL) (Fig. 3a and b). The BDC precipitate after the FDC and toward the centers of the pores. They tend to have brighter crystals 0.05–0.08 mm in diameter and exhibit a dull red color under CL (Fig. 3c and d).

The silt-to fine-sized crystalline dolomite cements (CD2) mostly occur along the edges of the pores, with relatively bright parallel crystals with diameters of 0.1–0.2 mm and with a dull red color under CL (Fig. 3e, f, i, j).

The medium-to coarse-sized crystalline dolomite cements (CD3) precipitate after the CD2 in the pores. The CD3 cements have larger-sized crystals with diameters of 0.25–1 mm toward the pore centers (Fig. 3e—h). The CD3 cements are mostly composed of the euhedral to subhedral dolomite crystals with a zonation from bright to dull red under CL.

The bright white saddle dolomite (SD) commonly precipitates in the centers of the vugs or fractures, with a curved crystal boundary, undulatory extinction under crossed polarized light and bright red colour under CL (Fig. 3g, h, k, l).

Two classes of silicification of the Deng-2 Member occur within the Penglai area. The first class is dominated by dispersed subhedral quartz which replace the dog-teeth-like dolomite cement (QZ1) (Fig. 4a and b). Euhedral or subhedral conical quartz (QZ2) can occur together with SD in the centers of vugs and fractures (Fig. 4c-g) with a dark color under CL (Fig. 31).

The other euhedral to subhedral crystalline cements such as sphalerites (Fig. 4j), fluorite (Fig. 4h and i), galenite, chalcopyrite, and barite have also been identified within the vugs and fractures, together with SD and quartz.

A large volume of solid bitumen has been observed adhering on the crystalline surface of CD2, CD3 and QZ2 within the pores, vugs, fractures and stylolites. The bitumen occupies the edge area of the vugs in the cores of Penglai area. Two types of solid bitumen have been observed under the microscope. One type is a continuous or discontinuous bitumen film (SB1) (Fig. 4k). The other type has a patchy or blocky distribution with a size of 1–2 mm (SB2) (Fig. 4l). The SB1 is mostly present on the surface of the CD2 within the

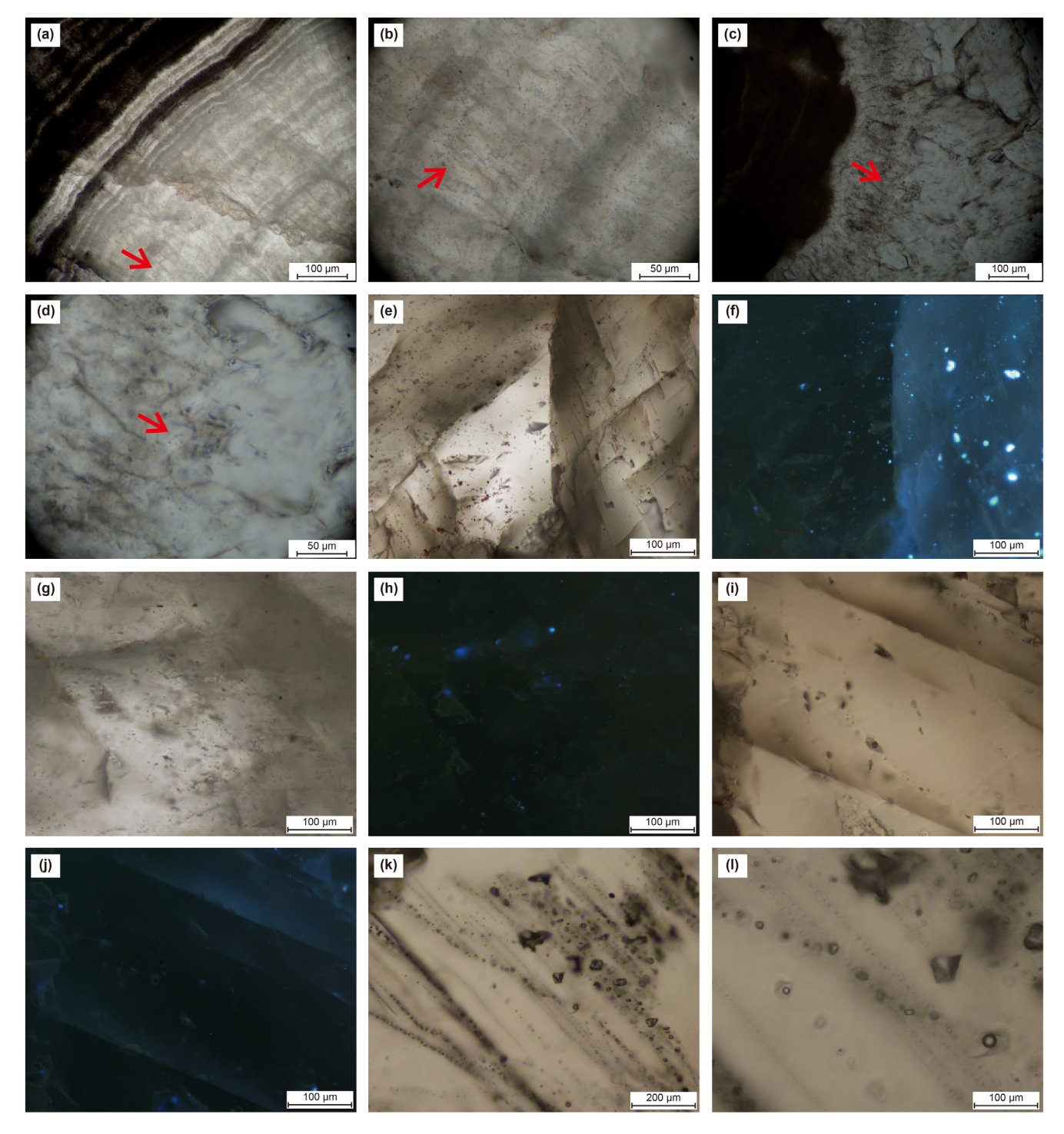


Fig. 5. Different types of cements and fluid inclusions in the Deng-2 Member, Penglai area.

(a) PT1 well, 5779.8m, fluid inclusion in FDC, PPL; (b) PT1 well, 5779.8m, fluid inclusion in FDC, PPL; (c) PT102 well, 5881.86m, fluid inclusion in BDC, PPL; (d) PT102 well, 5881.86m, fluid inclusion in BDC, PPL; (f) Fluorescence of (e), with some hydrocarbon fluid inclusions emitting blue light; (g) PT102 well, fluid inclusion in CD3, PPL; (h) Fluorescence of (g), with some hydrocarbon fluid inclusion in SD, PPL; (j) Fluorescence of (i), with some hydrocarbon fluid inclusions emitting, blue light; (k) PT102 well, QZ2 two-phase fluid inclusion, PPL; (l) PT102 well, QZ2 gas-liquid two-phase fluid inclusion, PPL: PPL: plane-polarized light.

pores or fractures while SB2 occurs on the surface of the CD3 in the center part of the vugs.

4.1.3. Mineral cementation parasequence

The first generation of cements such as FDC and BDC, occurs along the margins of the pores or vugs within the microbial mound

reservoirs of the Deng-2 Member, with fibrous isopachous linings and a dull red color under CL illumination (Fig. 3a—d). Subsequently, QZ1 is precipitated during the penecontemporaneous diagenetic phase, with dispersed or subhedral quartz replacement in occurrence (Fig. 4a and b). Precipitation of the CD2, which has a dull red color under CL occurs after QZ1 cementation (Fig. 3e and f).

Small amounts of bitumen SB1 can adhere to surface as a continuous or discontinuous bitumen film (Fig. 3i).

Subsequently, CD3 cements precipitate into the vugs with light and dark micron-thick laminations visible under CL (Fig. 3e—h). Precipitation of CD3 cements is followed by deposition of medium-to coarse-sized blocky solid bitumen (SB2) (Fig. 3k and 1). Precipitation of the last generation of dolomite cements is characterized the occurrence of SD in the pores or vugs with a curved crystalline boundary, undulatory extinction and a bright red colour under CL (Fig. 3g, h, k, l). In addition, Mississippi Valley Type (MVT) deposits, such as sphalerites (Fig. 4j), fluorite (Fig. 4h and i), can occasionally be found after the SD precipitation. Finally, coarse grain size euhedral or subhedral conical quartz (QZ2) squeeze the SD in the vugs (Fig. 4c—f, g).

4.2. Geochemical composition and properties

4.2.1. Trace elements and REE

Thrombolites (average (av.) = 581.42 ± 253.78 ppm (σ , standard deviation), n=3), stromatolites (av. = 427.48 ± 322.77 ppm, n=3), spongiostromata dolostone (av. = 338.67 ± 72.28 ppm, n=3), dolopackstone-dolograinstone (av. = 219.95 ± 26.10 ppm, n=4), dolowackestone-mudstone (av. = 342.96 ± 24.90 ppm, n=4), FDC (av. = 697.17 ± 367.07 ppm, n=10) and BDC (av. = 395.35 ± 277.19 ppm, n=11) have lower Fe content compared to CD2 (av. = 1865.46 ± 816.09 ppm, n=11), CD3 (av. = 1600.65 ± 100.06 ppm, n=12), and SD (av. = 3372.93 ± 1458.67 ppm, n=9) (Tables S1 and S2).

The Na content of the matrix tends to increase sequentially from thrombolites (av. = 247.25 \pm 17.38 ppm, n = 3), stromatolites (av. = 237.99 \pm 103.17 ppm, n = 3), spongiostromata dolostone (av. = 346.72 \pm 19.51 ppm, n = 3), dolopackstone-dolograinstone (av. = 459.11 \pm 49.35 ppm, n = 4) to dolowackestone-mudstone (av. = 612.00 \pm 49.34 ppm, n = 4), whereas into the cements, the Na content of CD2 (av. = 412.44 \pm 210.77 ppm, n = 11) and CD3 (av. = 260.19 \pm 171.28 ppm, n = 12) is much greater than that of FDC (av. = 189.69 \pm 41.36 ppm, n = 10), BDC (av. = 139.61 \pm 27.39 ppm, n = 11) and SD (av. = 91.96 \pm 29.25 ppm, n = 9).

Within the matrix, the Mn content of the microbialites such as thrombolites (av. = 437.30 ± 67.73 ppm, n=3), stromatolites (av. = 387.39 ± 32.33 ppm, n=3), and spongiostromata dolostone (av. = 356.86 ± 37.47 ppm, n=3) is significantly higher than that of dolopackstone to dolograinstone (av. = 225.37 ± 32.60 ppm, n=4) and dolowackestone to mudstone (av. = 163.42 ± 70.32 ppm, n=4). For the cements, the Mn content within the FDC (av. = 264.52 ± 90.77 ppm, n=10), BDC (av. = 174.19 ± 83.71 ppm, n=11) and CD2 (av. = 210.56 ± 67.26 ppm, n=11) is greatly lower than that in the CD3 (av. = 400.43 ± 54.12 ppm, n=12) and SD (av. = 800.47 ± 193.15 ppm, n=9).

In the matrix, the Sr content of thrombolites (av. = 72.56 ± 7.85 ppm, n = 3) and dolowackestone to mudstone (av. = 62.89 ± 21.90 ppm, n = 4) are significantly lower than that of stromatolites (av. = 95.81 ± 14.63 ppm, n = 3), spongiostromata dolostone (av. = 81.38 ± 14.34 ppm, n = 3), and dolopackstone to dolograinstone (av. = 88.97 ± 22.08 ppm, n = 4). For the cements, the FDC (av. = 60.66 ± 12.87 ppm, n = 10), BDC (av. = 54.19 ± 8.63 ppm, n = 11), and CD2 (av. = 55.25 ± 16.88 ppm, n = 11) are similar to the bulk rock but are higher than the CD3 (av. = 31.16 ± 1.33 ppm, n = 12) and SD (av. = 29.39 ± 4.54 ppm, n = 9) in Sr content.

The REEs patterns of the matrix, FDC, and BDC are characterized by Ce negative anomalies (av. = 0.73 ± 0.21 ppm, n = 38), slightly positive Gd anomalies (av. = 1.39 ± 0.73 ppm, n = 31), and super-chondritic Y/Ho ratios (av. = 48.77 ± 11.60 ppm, n = 38). CD2 shows several characteristics in REEs pattern such as Y/Ho

ratios (av. = 76.71 ± 41.91 ppm, n = 11) and of Nd - Pr enriched types within the CD2. And the CD3 shows several characteristics in REEs pattern such as largely positive Eu anomalies (av. = 2.89 ± 1.60 ppm, n = 8), strongly positive Y anomalies and heavy REE depletions while the SD changes into the REEs pattern of prominent positive Eu anomalies (av. = 9.71 ± 3.21 ppm, n = 8), and lower Y/Ho ratios (av. = 26.61 ± 5.99 ppm, n = 7) (Tables S2 and S4).

4.2.2. Carbon, oxygen and strontium isotope data

A increasingly negative trend in δ^{18} O has been present in the series from the matrix (av. $= -3.4 \pm 1.0$ %, n = 21), FDC (av. = -3.3 ± 1.2 %, n = 11), BDC (av. = -3.9 ± 1.5 %, n = 13), CD2 (av. = -6.9 ± 1.8 %, n = 16), CD3 (av. = -9.3 ± 0.6 %, n = 17), to the SD (av. = -11.2 ± 1.2 %, n = 13). The group of the matrix (av. = 2.5 ± 0.6 %, n = 21), FCD (av. = 2.9 ± 1.4 %, n = 11) and BCD (av. = 2.8 ± 1.0 %, n = 13) is greatly more positive than the other group of the CD2 (av. = $1.1 \pm 0.4\%$, n = 16), CD3 (av. = $0.4 \pm 0.5\%$, n = 17), and SD (av. = 0.6 ± 1.0 ‰, n = 13) in the δ^{13} C values. 87Sr/86Sr within However, the ratio the (av. \pm 0.000269, n = 5), and 0.710119 (av. = 0.713550 ± 0.001283 , n = 4) are significantly larger than that of the matrix (av. = 0.709082 ± 0.000155 , n = 21), FCD (av. = 0.709128 ± 0.000045 , n = 3), BCD (av. = 0.709120 ± 0.000018 , n = 3) and CD2 (av. = 0.709142 \pm 0.000025, n = 5) (Tables S5 and S6).

4.2.3. Fluid inclusions analysis

The fluid inclusions in diameter of 3-25 um are broadly distributed in FDC, BDC, CD2, CD3, SD and OZ2, in elliptical, circular, long-bar, approximately square or irregular shapes, in gas/liquid ratio of smaller than 20 % (Fig. 5, See supplementary material for further details). The gas-liquid two-phase inclusions in size of 3-5 µm have been mostly founded in the FDC (Fig. 5a and b) and BDC (Fig. 5c and d). The liquid oil inclusions mostly occur in CD2 and CD3, in dark or yellow brown color under a polarized microscope (Fig. 5e-g) and in blue color under a fluorescence microscope (Fig. 5f-h). However, the gas phase methane inclusions in size of $9{-}20\,\mu m$ have been mostly recognized within the CD3, SD and QZ2, which are together with the saline inclusions in color of gray under a polarized microscope (Fig. 5i-1). The Th shows an increasing trend from FDC (Th = 52.7-65.2 °C, n = 18), BDC $(Th = 76.4 - 98.5 \,^{\circ}\text{C}, n = 23), CD2 \,(Th = 103.4 - 150.2 \,^{\circ}\text{C}, n = 97), CD3$ (Th = 138.9–184.3 °C, n = 89), SD (Th = 177.5–243.6 °C, n = 55) to QZ2 (Th = 162.2-217.3 °C, n = 35). However, the freezing temperatures (Tm) of FDC (Tm = -3.4--0.8 °C, n = 18), BDC $(Tm = -8.6 - -4.2 \, ^{\circ}\text{C}, \, n = 23), \, SD \, (Tm = -15.7 - -0.5 \, ^{\circ}\text{C}, \, n = 55)$ and QZ2 (Tm = -6.4-0.3 °C, n = 35) are much larger than that of CD2 (Tm = -21.3 - 4.2 °C, n = 97) and CD3 (Tm = -25.4 - -1.2 °C, n = 89) (Table S7).

4.2.4. Quantitative distribution of cementation in pores, vugs and fractures

A total of 152 pores and 93 fractures have been identified, including 72 completely cemented pores and 62 totally filled fractures. Based on the reorganization of the final generation of cementation, the vugs, pores and fractures have been divided into FDC-, BDC-, CD2⁻, CD3⁻, SD-, and QZ2-cemented types in detail, as well as non-cemented ones. QZ1 occurs less frequently and is not evaluated in this study. The proportion of the FDC-BDC-cements, the CD2-cements, CD3-cements, SD-cements and QZ2-cements in completely cemented pores and vugs is respectively 11.11%, 5.56%, 56.94%, 18.06% and 8.33%. However, in the incompletely cemented vugs and pores, the FDC-BDC-cements, CD2-cements, CD3-cements, SD-cements and QZ2-cement are 6.25%, 6.25%, 56.25%, 16.25% and 12.5% of the volume respectively with a non-cemented

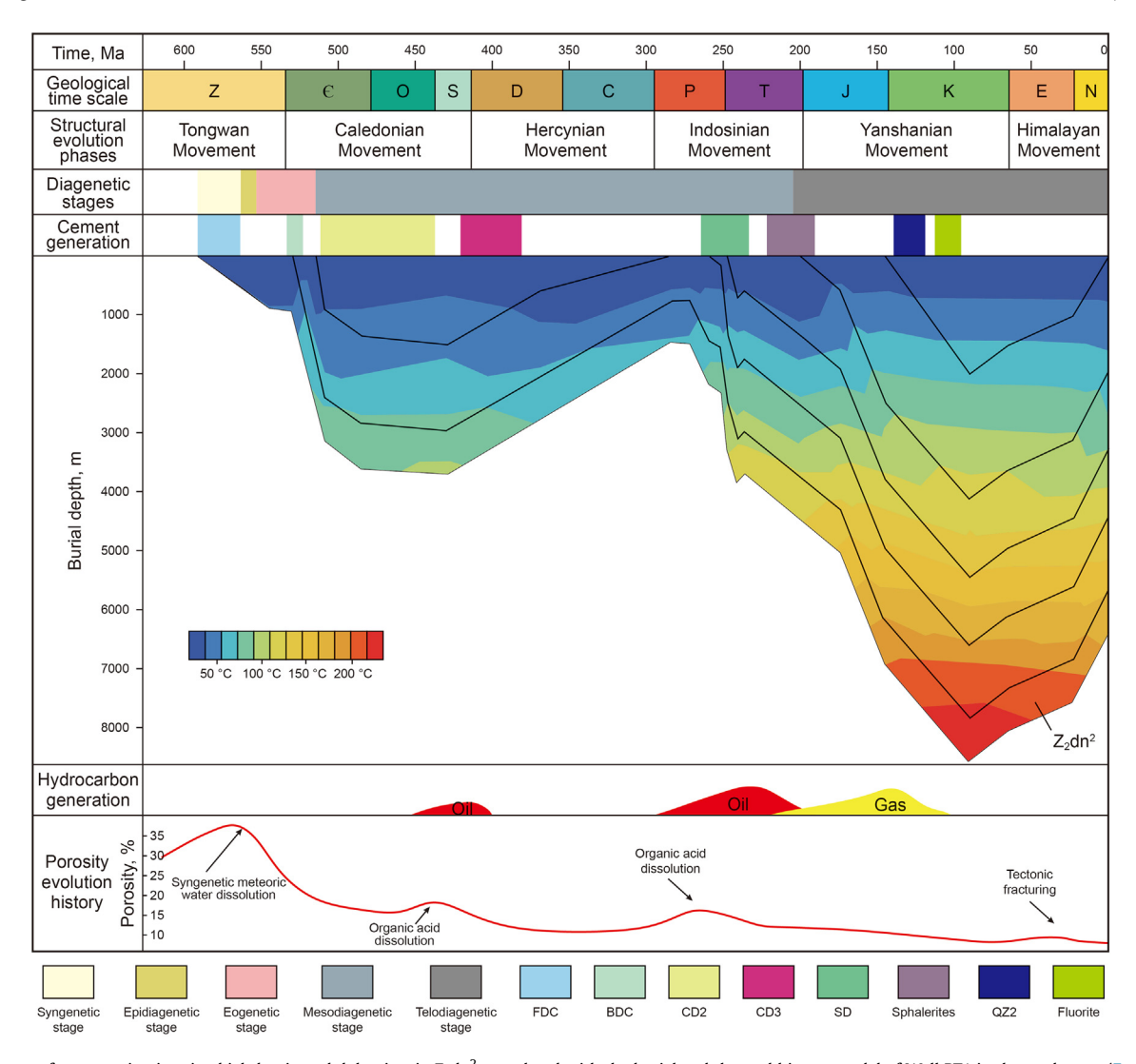


Fig. 6. Sequence of cementation in microbial-dominated dolomites in Z_2dn^2 , correlated with the burial and thermal history model of Well PT1 in the study area (Fan et al., 2022; Shen et al., 2021).

volume of 2.5%. The values here represent the frequency of the sample.

In the totally cemented fractures, the CD3-cements, SD-cements and QZ2-cements constitute 79.03%, 12.9% and 8.06% respectively of the total volume. In contrast, they are 48.39%, 16.13% and 9.67% of the volume within the incompletely cemented fractures. However, there are no FDC-BDC and CD2 cements in both the totally and incompletely cemented fractures. The non-cemented volume in the fractures is 25.81%.

5. Interpretation and discussion

5.1. Paleofluids evolution within the ultra-deep microbialite reservoirs of the Deng-2 member

The multiple episodes of exposure, dissolution, and precipitation that occurred during the major uplift events over the past 500 million years have resulted in a high degree of heterogeneity in the microbialite reservoirs in the Deng-2 Member. Penecontemporaneous karstification occurs when the shallow water microbialites are subaerially exposed during the sea level falls, resulting in the formation of inter-clot pores and microbial fenestral pores.

During the Tongwan phase in the upper Yangtze block, two tectonic uplift episodes occurred, leading to the formation of regional unconformities at the top of the Deng-2 Member and Dengying Formation (Li et al., 2015). These uplift events also triggered extensive epigenetic karstification. As a result, a large number of pores and vugs were formed, significantly enhancing the reservoir quality (Tang et al., 2013). Furthermore, the hydrocarbon generation and cracking processes generated fluids rich in organic acids, carbon dioxide, and hydrogen sulfide. These fluids contributed to the improvement of reservoir properties. The five diagenetic stages have been recognized such as syngenetic, epigenetic, eogenetic, mesogenetic and late diagenetic within the Deng-2 Member, according to the paleofluid types, burial and thermal evolution history (Li et al., 2014; Fan et al., 2022) (Fig. 6).

5.1.1. Syngenetic stage

In the late Ediacaran period, the Sichuan Basin was located at approximately 30 °N in latitude and was covered by a shallow sea with a temperature of ~20 °C–25 °C (Scotese, 2009; Meng et al., 2011). Large scale syngenetic dolomitization occurred on the platform as a result of strong evaporation in a restricted circulation environment as well as the lower dynamic barrier related to the

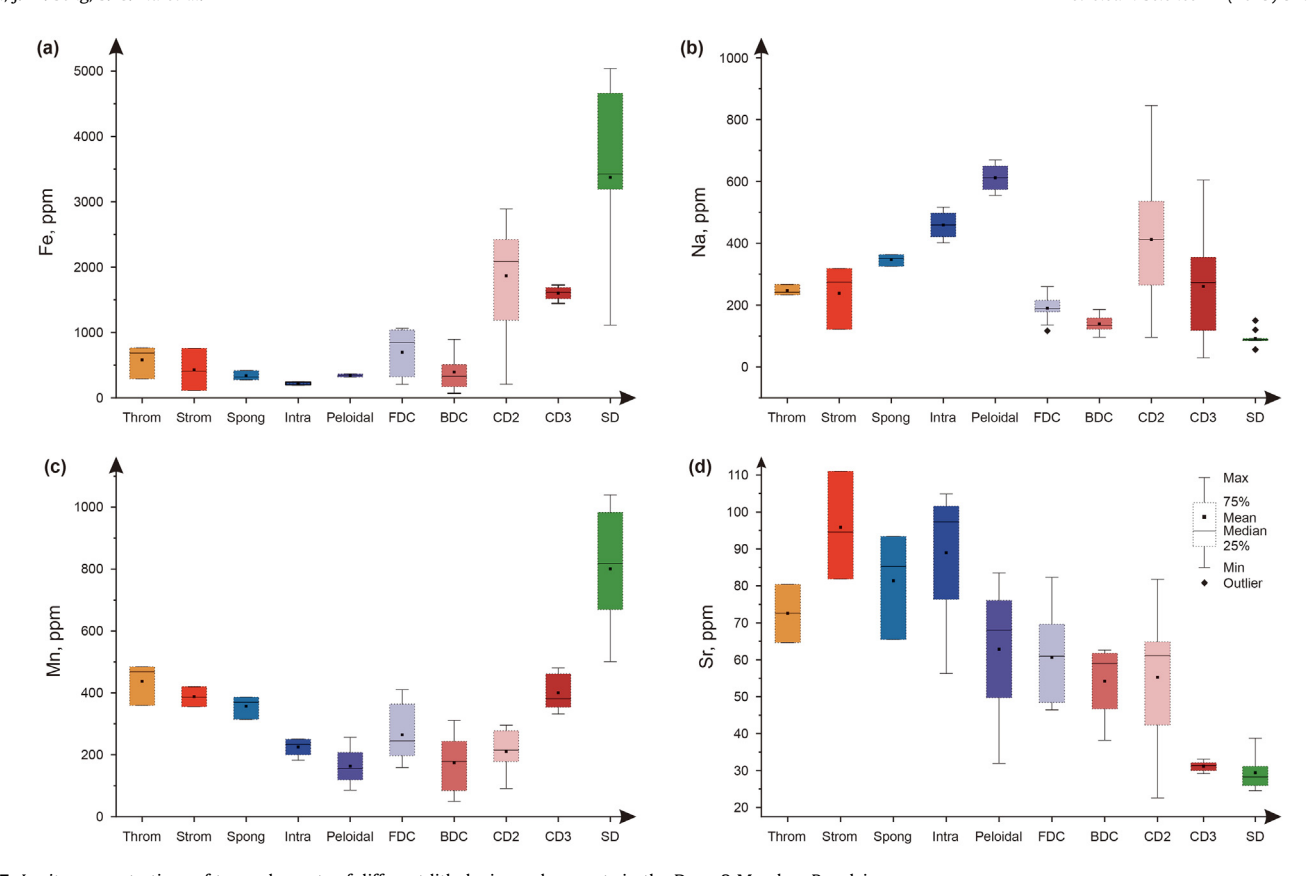


Fig. 7. *In situ* concentrations of trace elements of different lithologies and cements in the Deng-2 Member, Penglai area. **(a)** Fe concentration; **(b)** Na concentration; **(c)** Mn concentration; **(d)** Sr concentration. Throm = Thrombolites, Strom = Stromatolites, Spong = Spongiostromata dolostone, Intra = Intraclastic dolopackstone-grainstone, Peloidal = Peloidal dolowackestone-mudstone.

microbe flourishing (Sánchez-Román et al., 2009; Petrash et al., 2017; Zhao et al., 2020), which led to the preservation of the microbial fabrics and of information on the composition of the paleoseawater. The trace element compositions such as lower concentrations of Fe and Mn, higher concentrations of Na and Sr, a pattern of heavy REE (HREE) enrichment, and higher Y/Ho ratios are similar to those of upper Ediacaran carbonates in Brazil (Paula-Santos et al., 2020) (Figs. 7 and 8). In addition, the δ^{13} C (1.41 ‰– 3.68 %, n = 21, av. = 2.55 %), δ^{18} O (-5.85 % to -1.32 %, n = 21, av. = -3.42 %) and δ^{18} O (0.708837–0.709313, δ^{18} O (0.708837–0.709313, δ^{18} O (0.708837–0.709313). av. = 0.709082) of the microbial dolostone are mostly within the ranges of the late Ediacaran seawater ($\delta^{13}C=0$ %–5 %, $\delta^{18}O=-2.4$ $\% \sim -6.8 \,\%$, 87 Sr/ 86 Sr = 0.70908-0.70937) (Burns et al., 1994; Jiang et al., 2007; Tahata et al., 2013), indicating the seawater-sourced fluids for dolomitization (Fig. 9). However, additional volumes of pores and vugs were produced in the Deng-2 Member microbialite reservoirs during the penecontemporaneous syngenetic stage due to frequent eustatic cycles (Ding et al., 2019).

When the exposed microbialite reservoirs flooded, seawater reentered the framework pores in the thrombolites and stromatolites, fenestral pores in the lamination and the penecontemporaneous karstification vugs are filled. At this time FDC cementation along the margin of the pores and vugs as the burial depth, temperature and pressure increased, which also preserved the information on the composition of the paleoseawater. The ranges of the concentrations of trace elements such as Fe, Na, Mn, and Sr are similar to the those of the matrix of the microbialites (Fig. 6), as are the HREE enrichment patterns (Fig. 7). Additionally, the δ^{13} C (0.46 %–4.85 %), δ^{18} O (–1.16 % to –4.62 %) and δ^{13} C ratios (0.709083–0.709173) are also within the ranges of isotope ratios

for late Ediacaran seawater (Fig. 9). The Th of fluid inclusions within FDC are 52.7 °C—65.2 °C and the salinities vary from 1.46% to 5.47%, which also suggest a seawater source (Figs. 10 and 11a).

5.1.2. Epigenetic diagenetic stage

The first uplift episode of the Tongwan tectonic phase led to the large-scale subaerial exposure of the top of the Deng-2 Member (Zhu et al., 2019), resulting in epigenetic karstification and formation of features such as karst breccia, cave collapse breccia, and vadose silts. The paleofluids were dominated by a mixture of meteoric freshwater and seawater (Fig. 11b).

5.1.3. Eogenetic diagenetic stage

In the BDC, the framework pores, inter-clot pores and vugs began to be cemented after the rapid burial of the Deng-2 Member strata in the early Cambrian, when an extensive transgression occurred (Zhou et al., 2017). Consequently, the concentrations of trace elements such as Na (96.33-185.44 ppm, av. = 139.61 ppm), Mn (49.15-311.41 ppm, av. = 174.19 ppm), Fe (70.81-896.02 ppm,av. = 395.35 ppm), and Sr (38.18-72.63 ppm, av. = 57.83 ppm) are much lower in the BDC than in the FDC (Fig. 7), which indicates that the paleofluids of BDC were still being influenced by meteoric freshwater. However, the HREE enrichment pattern in the BDC is similar to that in the FDC (Fig. 7). In comparison with the composition of the late Ediacaran seawater, the BDC has slightly more negative δ^{18} O (Fig. 9a) values. The fluid inclusion Th values of 76.4-98.5 °C and salinities of 6.64%-12.40% in salinity, which indicate a shallow burial environment (2000–3000m) (Fig. 11b). At the same time, the re-precipitation of the material dissolved by meteoric water can also lead to higher salinity of inclusions in BDC

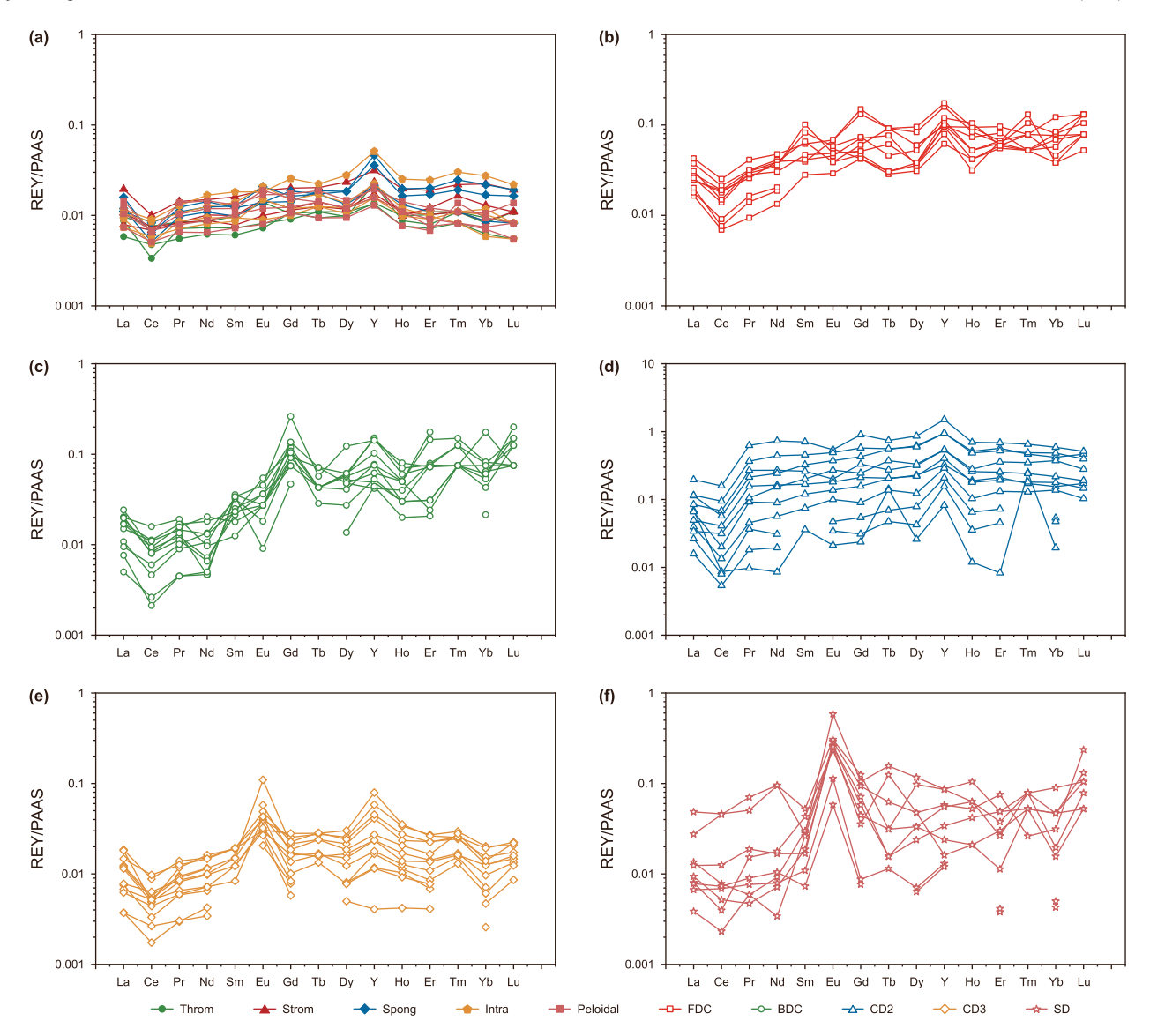


Fig. 8. *In situ* REY distributions of different lithologies and cements in the Deng-2 Member, Penglai area. Throm = Thrombolites, Strom = Stromatolites, Spong = Spongiostromata dolostone, Intra = Intraclastic dolopackstone-grainstone, Peloidal = Peloidal dolowackestone-mudstone.

than in FDC. The selective silicification occurred within the fenestral pores of the microbial framework as small-sized fibrous quartz (QZ1). This phenomenon may be attributed to the residual seawater present in the original pores (Wang et al., 2022).

5.1.4. Mesogenetic diagenetic stage

As the burial depth increases to ~4000m, the interval temperatures and overpressure coefficients reach $120\,^{\circ}\text{C}-150\,^{\circ}\text{C}$ and 1.2 to 1.5 respectively (Fan et al., 2022), at which point CD2 begins to precipitate on the surface of BDC. The trace concentrations of the CD2 are as follows: Na (95.96–845.89 ppm, av. = 412.44 ppm), Mn (90.90–295.56 ppm, av. = 210.56 ppm), Fe (208.81–2889.16 ppm, av. = 1865.46 ppm), and Sr (22.58–81.75 ppm, av. = 55.25 ppm), which show higher concentrations of Fe and Mn compared to the matrix, FDC and BDC (Fig. 7).

However, a MREE-enriched pattern occurs in the CD2 (Fig. 8). The isotopic ratios δ^{13} C (0.1 ‰–1.8 ‰), δ^{18} O (–4.1 ‰ – –9.8 ‰), δ^{87} Sr/ δ^{86} Sr ratio (0.709114 - 0.709169) within the CD2 (Fig. 9), are more negative δ^{18} O than paleoseawater. In addition, the Th of the fluid inclusions range from 103.4 °C to 150.2 °C and the salinity

varies from 6.64% to 23.05% (Figs. 10 and 11c), both of which suggest an estimated burial depth of 3000 m–4000 m (Fig. 6). Consequently, the formation fluids are differences in the δ^{18} O, Fe-Mn and REE distribution patterns from the paleoseawater and are mostly the result of the burial thermal fractionation of oxygen isotopes and some certain trace elements (Fe, Mn and Sr) concentration.

The first hydrocarbon charge episode responsible for SB1 follows the CD2 and is related to expulsion of petroleum from the Qiongzhusi Formation in the late Silurian to Devonian period (Shen et al., 2021). This is demonstrated by the bitumen films on the edges and the hydrocarbon fluid inclusions inside the CD2 cements (Fig. 11). However, SB1 does not occur extensively within Penglai area, suggesting only the small volume of expelled petroleum. The CD3 does not occur until the end of the first hydrocarbon expulsion episode (SB1). The trace element concentrations of CD3 indicate a significantly higher concentration of Mn and lower concentrations of Sr in comparison with the matrix, FDC, BDC and CD2 (Table S1, Fig. 7). The REE distribution pattern is similar to the pattern of typical low-temperature hydrothermal fluids (Fig. 8), with much small δCe negative anomaly, obvious δEu positive anomaly, as well

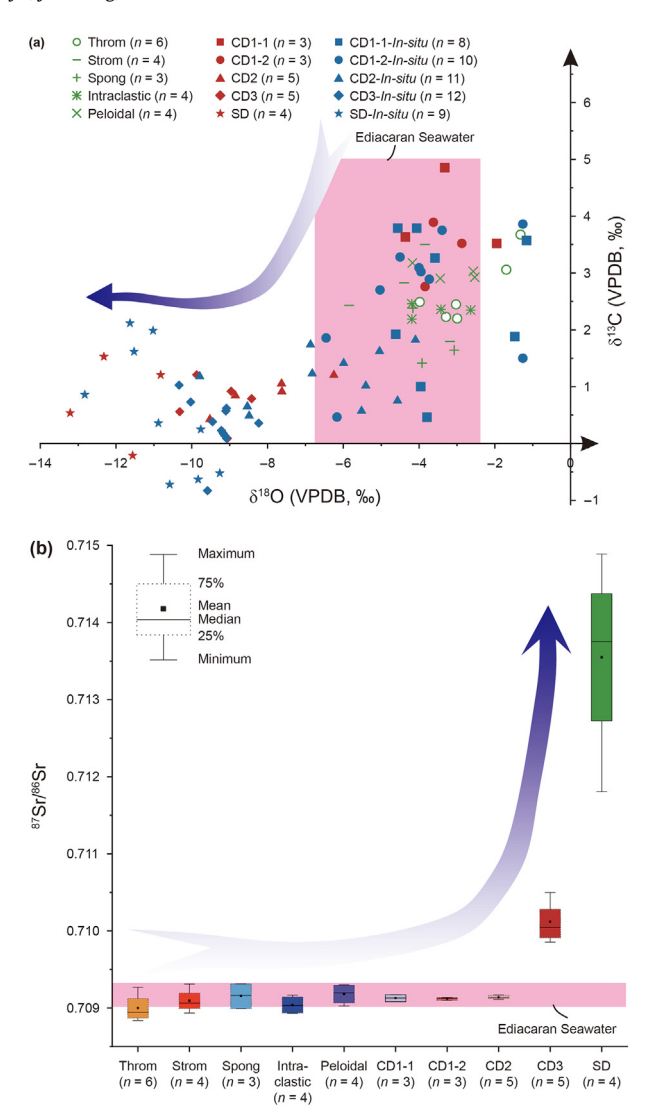


Fig. 9. (a) Scatterplot of δ^{13} C versus δ^{18} O of the different lithologies and cement in the Deng-2 Member, Penglai area; (b) 87 Sr 78 Sr ratios of different lithologies and cements in the Deng-2 Member, Penglai area.

as the smaller concentrations of total REE (Bau and Dulski, 1996). In addition, the isotope ratios of the CD3 as negative δ^{13} C (0.1 ‰–1.2 ‰) and δ^{18} O (-10.3 ‰ -8.2 ‰), and δ^{7} Sr/ δ^{8} Sr ratios are large (0.709855 - 0.710500) (Fig. 9), which indicate a stable closed diagenetic system at relatively high temperatures. This interpretation is consistent with the relatively high Th values (138.9 °C–184.3 °C) and fluid inclusion salinities (2.10%–24.59%) of the fluid inclusions in CD3 (Figs. 10 and 11c).

It has been proposed that the CD3 was precipitated from lower-temperature hydrothermal fluids in a relatively closed diagenetic system from the late Silurian to Devonian, as indicated by considering the characteristics of the REE-Y distributions, negative δ^{18} O, higher Th values, as well as the U-Pb dating results (Shen et al., 2021). Consequently, it is suggested that the thrusting that occurred in the late Silurian Caledonian orogeny resulted in ultradeep thermal brines, which are enriched in 18 O, being injected into Deng-2 Member reservoirs by migrating along the nearly vertical strike-slip fault zone formed in the early Cambrian and the along the unconformity surface at the top of the Deng-2 Member.

A second hydrocarbon generation and expulsion event occurred

after precipitation of CD3, with the SB2 being deposited as dispersed particles or flakes in the inter-crystalline pores (Fig. 11c). This event probably represents the peak hydrocarbon expulsion episode of the Qiongzhusi Formation source rock in the late Permian to Triassic period (Ni et al., 2020). In addition, the abundance of oil-gas fluid inclusions within the CD3 is consistent with the occurrence of extensive petroleum expulsion and migration at that time, with quantities of bitumen left after cracking (Fig. 11).

5.1.5. Late diagenetic stage

The saddle dolomite (SD) precipitates in the central part of the pores and vugs after the SB2 (Fig. 11d). Compared with the previous generations of cements, the SD cements have much higher concentrations of Fe and Mn, and lower concentrations of Na and Sr (Table S3, Fig. 7) In addition, SD cements have significantly more positive δEu anomalies in the REE distribution pattern (Table S4, Fig. 8). Isotopically, the most negative $\delta^{13}C$ (-0.7% to -2.1%) and $\delta^{18}O$ (-13.2 % to -10.8 %), and highest ${}^{87}Sr/{}^{86}Sr$ ratios (0.711806 - 0.714887) occur in the SD (Fig. 9). Similarly, the Th values range from 177.5 to 243.6 °C and the salinities from 0.97% to 19.45% for the fluid inclusions in SD (Figs. 10 and 11c), which has an estimated burial depth of ~4500m (Fig. 6), with a maximum burial temperature of ~230 °C (Hu et al., 2020b). The most negative δ^{13} C (-0.7 % to -2.1 %) are explained as mixing of preexisting inorganic CO₂ with TSR-derived CO₂ as reported from the other TSR provinces (Cai et al., 2001, 2003, 2004, 2014; Liu et al., 2016a) while the highest 87 Sr/ 86 Sr ratios and the much lower δ^{18} O values than other cements may be related to crustal-derived fluids originating from the upwelling E'meishan mantle plume (also called 'E'meishan Large Igneous Province') (Su et al., 2022). In addition, other cementation minerals such as sphalerites and fluorite have also been identified in the reservoirs in the Deng-2 Member. It has been proposed that hydrothermal fluids migrated upward along deep faults in the late Permian, as indicated by the radioisotope dating of Rb-Sr in sphalerite (Jiang et al., 2016; Shen et al., 2019; Zhang et al., 2019). This would have induced silicification at both a local and an extensive scale, together with TSR. The massive silicification is mostly adjacent to faults in the form of coarse columnar quartz (QZ2) as the hydrothermal fluids migrated along interconnected pores in the layered-dissolution pores and vugs (Fig. 11d).

5.2. Coupled effects of paleofluid evolution and ultra-deep microbialite reservoir modification

The complicated history of paleofluid compositions and their coupled effects on the heterogeneity of ultra-deep microbialite reservoirs in the Deng-2 Member have been lasting for more than 500 Ma. The original pore spaces from deposition developed mostly within thrombolites and stromatolites along the platform margin during the syngenetic diagenetic stage. However, early porous to vuggy porosity systems developed due to periodic high-frequency exposure and drowning events during the eustatic cycles and are the basis for the high-quality reservoirs of the Deng-2 Member. The onset of the Tongwan tectonic phase led to the uplift of the entire Yangtze block, and resulted in basin-scale karstification at the top surface of the Deng-2 Member in the epigenetic diagenetic stage, as well as the cementation of FDC and BDC. The FDC and BDC comprise 11.11% of the cement volumes in the totally cemented vugs and 6.25% of the volume in the partially cemented vugs (Fig. 12).

The CD2 and CD3 cements did not precipitate in the vugs until the mesogenetic diagenetic stage (Fig. 12), when the Deng-2 strata were gradually buried and fluid circulation decreased significantly. In the totally cemented vugs, the CD2 and CD3 occupy 5.56% and 56.94% respectively of the pore volume, while they occupy 6.25%

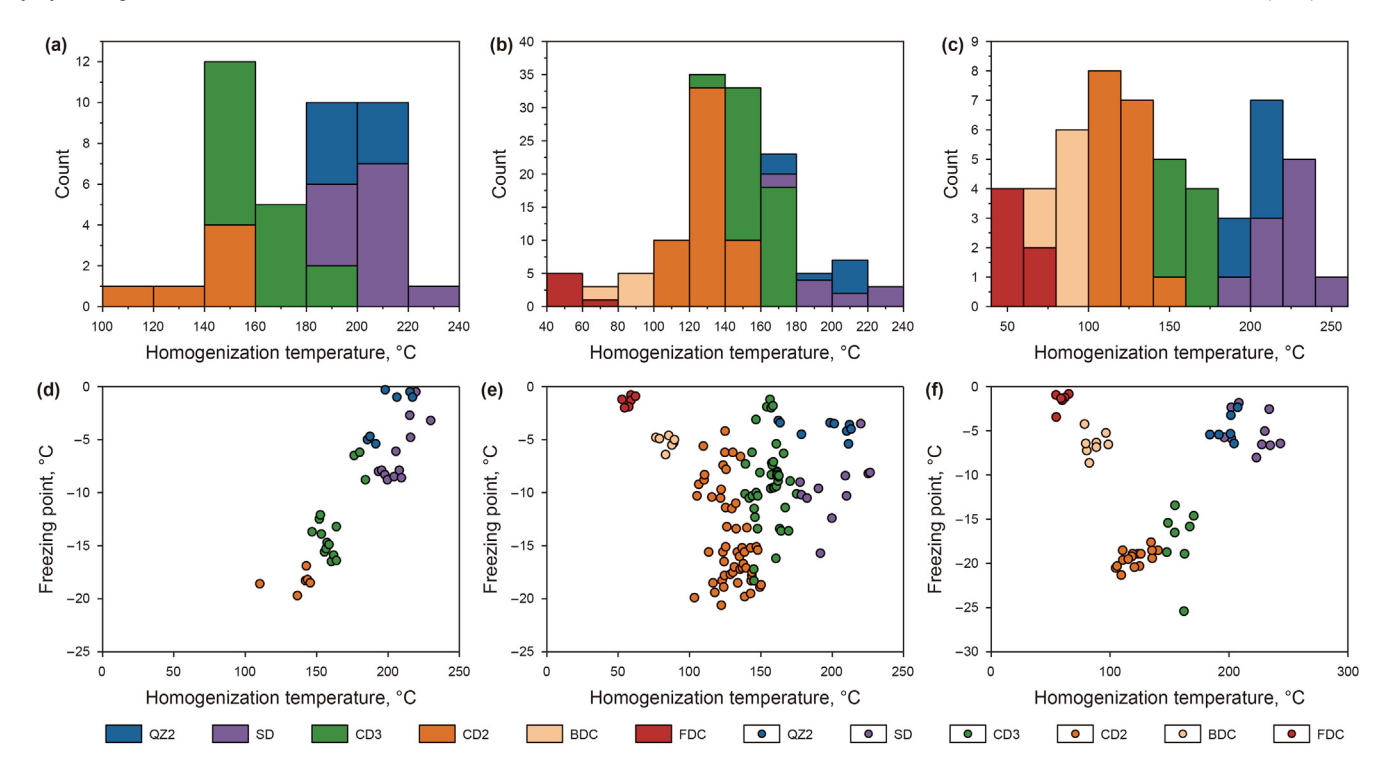


Fig. 10. Characteristics of fluid inclusions in cement in the Deng-2 Member, Penglai area. **(a)** and **(d)** data from Z[2; **(b)** and **(e)** data from PT1; **(c)** and **(f)** data from PT102.

and 56.25% respectively of the pore volumes in partially cemented pores and vugs. Although CD2 does not occur in the fractures, CD3 cements occupy 79.03% and 48.39% of fracture volume within the totally and partially cemented fractures respectively. This suggests that CD2 cementation had little negative impact on the reservoirs, which may be related to the two hydrocarbon charge episodes. Prior to the precipitation of CD3 cements, the reservoirs experienced large scale cementation due to the deep low-temperature hydrothermal fluids migrating along the strike-slip faults and the unconformity surfaces at the top of the Deng-2 Member during the Caledonian phase.

The SD and QZ2 cements related to the hydrothermal fluids of the E'meishan large igneous event were emplaced in the late diagenetic stage, when the paleofluids were confined in a relatively closed environment and would substantially reduce the residual porosity of the Deng-2 Member. However, multiple high angle and diagonal fractures generated by the Himalayan tectonic phase significantly connected the isolated pores and vugs, which improved the reservoir permeability of the Deng-2 Member. In addition, the SD and QZ2 account for 18.06% and 8.33% of the pore space of the totally cemented vugs and 16.25% and 12.5% of the volume of partially cemented vugs (Fig. 12). However, the SD and QZ2 make up 12.9% and 8.06% in volume within the totally and partially cemented fractures, respectively, while they are 16.13% and 9.67% in the partially cemented fractures. The non-cemented fractures represent 25.81% of the total of 93 fractures (Fig. 12).

These data indicate that two stage of paleofluid-driven diagenesis have occurred, based on the diagenetic products and their impact on reservoir quality. These are the syngenetic or penesyngenetic to the early extent of mesogenetic diagenesis, and the later period of mesogenesis to the late diagenetic stage. The FDC, BDC and CD2 are the diagenetic products of penesyngenetic karstification, epigenetic karstification and shallow burial cementation after hydrocarbon migration during the early period of mesogenetic diagenetic stage. The penesyngenetic karstification in

the microbialites will produce large numbers of pores and vugs and so enhance the reservoir quality during the succeeding epigenetic karstification, which in turn causes the disappearance of the FDC and BDC. Subsequently, hydrocarbon generation and migration occurs during the early period of mesogenetic diagenetic stage, which prevents the CD2 precipitation and further enhances dissolution and modification. Consequently, the paleofluid interactions in this stage are favorable for reservoir formation.

The CD3, SD and QZ2 were precipitated during later period of the mesogenetic to the late diagenetic stage and are related to the deep earth fluid activities. During the Caledonian period, deeply sourced hydrothermal fluids migrated along near-vertical strikeslip faults and the unconformity surface at top of the Deng-2 Member, resulting in precipitation of the CD3, which reduced reservoir quality, and offset the dissolution during the peak hydrocarbon migration episode. In contrast, late diagenetic processes, as reflected by precipitation of SD, were more positive for the reservoir quality. Comparisons of thin sections revealed that SD usually develops simultaneously with CD3 in high-quality reservoirs, with low plane porosity (~1%) where only CD3 precipitates without SD precipitation, while CD3 develops harbour-like dissolution with higher plane porosity (3-4%) when CD3 precipitates simultaneously with SD. The widespread silicification (QZ2) and TSR helped to preserve pores and vugs to a certain extent. Through the observation and statistics of core and thin section, the pores that precipitated QZ2 has a plane porosity of 5–7%, which is much larger than the average plane porosity (~3%). The prevalence of harbour-like dissolution on the surface of SD, the higher formation temperature (>180 °C) and negative carbon isotopes (~-1 ‰) are all proofs of the existence of TSR in this area (Cai et al., 2016), which is probably one of the important factors for the existence of ultradeep high-quality dolomite reservoirs in the Deng-2 Member. In addition, the large quantities of bitumen in the pores inhibited the entrance of hydrothermal fluids, as shown by the lack of cementation in the fractures during the Yanshanian to Himalayan

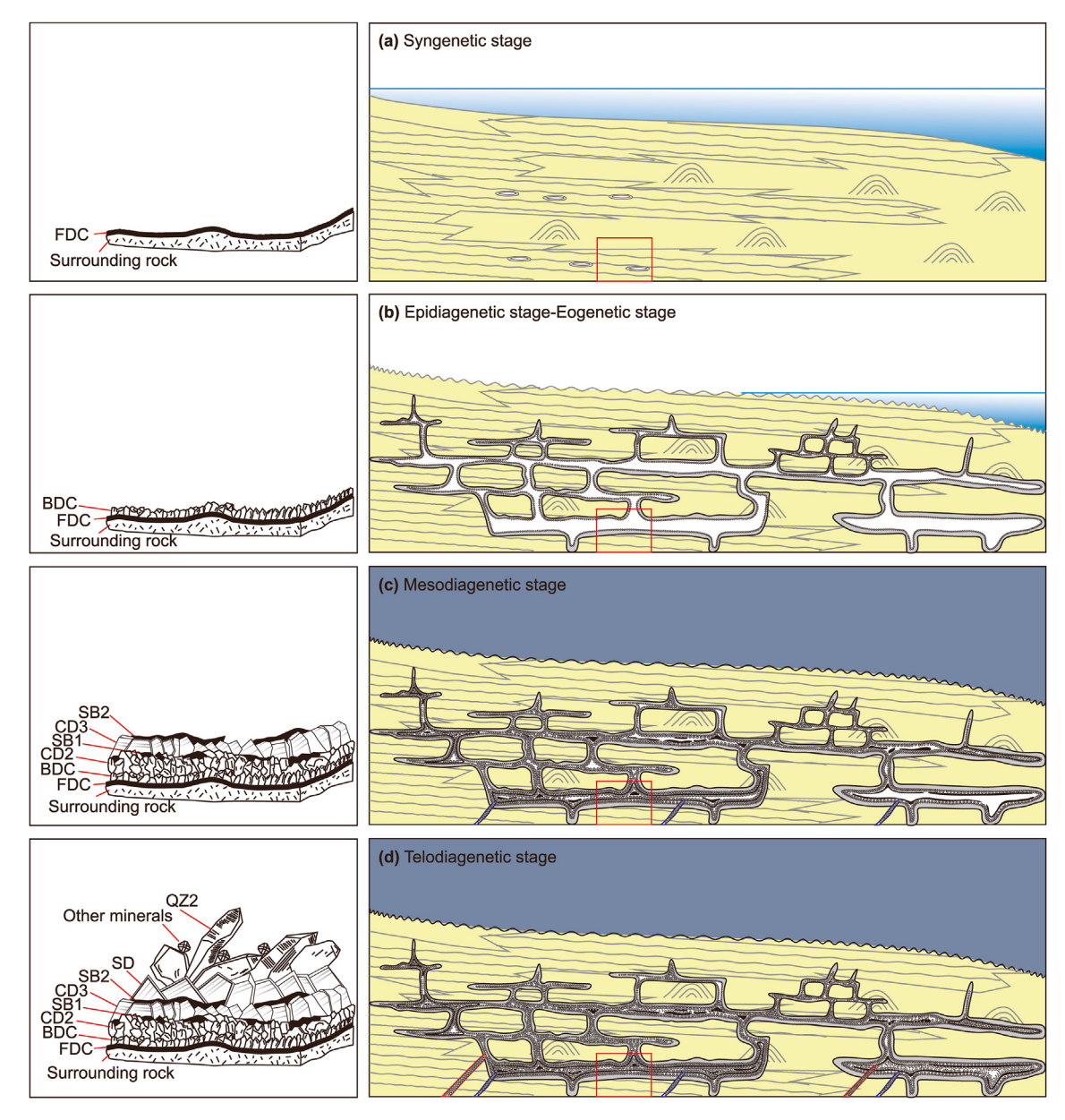


Fig. 11. Evolution model of paleofluids in the Deng-2 member, Penglai area.

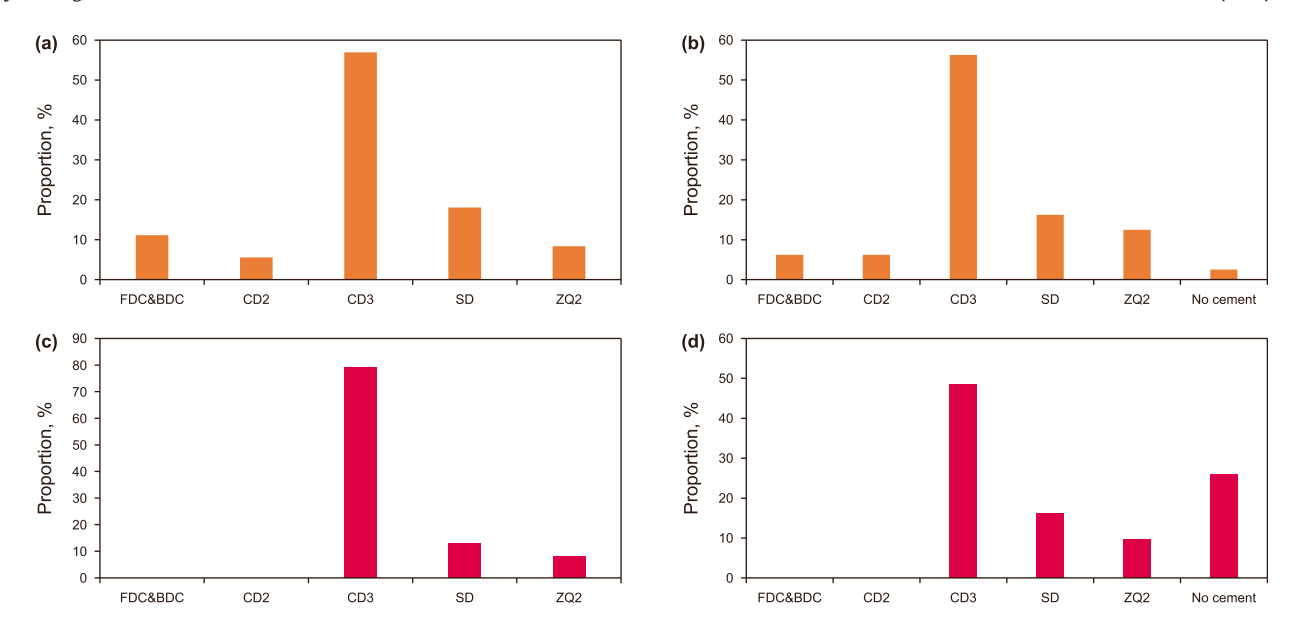


Fig. 12. Proportion of Cements in the Deng-2 Member, Penglai area.
(a) the pores are completely cemented; (b) the pores are incompletely cemented; (c) the fractures are completely cemented; (d) the fractures are incompletely cemented.

orogenic period.

Nowadays hydrocarbon exploration breakthroughs within the deep to ultra-deep carbonate reservoirs have been always updated (Han et al., 2019; Wei et al., 2022). The coupled effects of several stage of paleofluid evolution have been documented such as syngenetic dissolution, dolomitization, hydrothermal activities and burial variations (Conliffe et al., 2012; Liu et al., 2014; Kolchugin et al., 2020; Sun et al., 2023), which mutually result in the constructive or destructive modification to the reservoir porosity.

5.3. Implications for exploring ultra-deep microbialite reservoir plays

In China, microbialite reservoirs are mainly located in the Sichuan Basin, Tarim Basin, and North China Plateau, which are mainly characterised by low porosity and permeability. We compared the formation processes and patterns of deep-ultra-deep carbonate high-quality reservoirs in these basins, and found that the mechanisms of paleofluid activity in these reservoirs are similar (Table 1). In the early stages of sedimentation and diagenesis (Syngenetic-Eogenetic diagenetic stage), the paleofluids laid down the material foundation of the reservoirs, and also served as an important medium for dolomitization and quasi-symbiotic dissolution. With the occurrence of epigenetic karst, a large number of pores were formed and greatly improved the quality of the reservoir, which was a crucial paleofluid activity. In the mesogenetic diagenetic stage, the charging of hydrocarbon fluids contributes to reservoir preservation, but the dissolution and adjustment (mineral re-precipitation) of the reservoir by the paleofluids during this period leads to a decline in reservoir quality. In the late diagenetic stage, hydrothermal fluids, organic acids and TSR brought by strong tectonic movements broke the chemical balance within the original formation, constituting a new fluid environment, and remodelling the reservoir again, and at the same time, certain minerals (e.g., quartz) precipitated in this period have great compressive strength and stability, which is important for the preservation of the reservoir in the buried stage.

In summary, this study shows that the formation of high-quality reservoirs in the ultra-deep microbialite of these basins is the result of the coupling of sedimentation and diagenesis. Paleofluids played

different roles at different stages of reservoir evolution and were important for the porosity within the reservoirs. Our work suggests that paleofluids in the early and late diagenetic stages created favorable conditions for reservoir modification and preservation, and hydrocarbon fluids preserved porosity in the middle diagenetic stage. These findings have potential implications for other ultradeep microbial reservoirs.

6. Conclusions

- (1) There were nine stage of paleofluid activities in the microbialites reservoirs of the Deng-2 Member in the Penglai area, including five stage of dolomite cement such as FDC, BDC, CD2, CD3 and SD, selective silicification (QZ1) associated with early residual seawater in the original pores, two stage of hydrocarbon migration sourced from the black shales of the Qiongzhusi Formation in the late Silurian to Devonian (SB1) and late Permian to Triassic (SB2), and the siliceous cementation (QZ2) related to the influx of late Permian hydrothermal fluids.
- (2) In the microbialite complexes, large numbers of pores and vugs were generated during the syngenetic to parasyngenetic diagenetic stage due to the high-frequency cycles of exposure and submergence in marine environments. This resulted in a fibrous cement lining the pores (FDC). Subsequently, the microbialites continued to dissolve due to uplift during the first episode of the Tongwan tectonic phase. The bladed cements penetrated into the epigenetic karstification pores and vugs (BDC) in the early diagenetic stage. Although compaction, cementation (CD2 to SD) and silicification (QZ2) took place in order during mesogenetic to late diagenetic stage resulting in the substantial porosity loss, the reactions of paleofluids over multiple periods and with variable compositions have different effects on the reservoir quality. The FDC, BDC and CD2 growing in the early stages had little negative influence on the reservoir quality. However, large scale cementation of hydrothermal fluids along the strikeslip faults and the unconformity surface at top of the Deng-2 Member during the Caledonian period precipitated the CD3 and resulted in intensive reservoir destruction.

Paleofluid evolution of typical microbialite-dominated dolomite reservoirs in China.

Basin/Location	Sichuan Basin			Tarim Basin		North China platform
Stratigraphic interval Time Main reservoir lithology	Leikoupo Formation Middle Triassic Thrombolitic and stromatolitic dolomites	Deng-2 Member Upper Ediacaran Thrombolitic and stromatolitic dolomites	Deng-4 Member Upper Ediacaran Stromatolitic dolomites	Xiaoerbrak Formation Lower Cambrian Thrombolitic and stromatolitic dolomites	Oigebrak Formation Upper Ediacaran Stromatolitic dolomites	Wumishan Formation Mesoproterozoic Thrombolitic and stromatolitic dolomites
Sedimentary facies Main Syngenetic- paleofluid Eogenetic	Platform Penecontemporaneous dissolution-Paleoseawater,	Platform Penecontemporaneous Dissolution-Paleoseawater,	Platform Penecontemporaneous dissolution-Paleoseawater,	Ramp Platform Penecontemporaneous Penecontempo dissolution-Paleoseawater, Paleoseawater,	Platform Penecontemporaneous dissolution- Paleoseawater,	Ramp Penecontemporaneous dissolution-
stage diagenetic stage		Early dolomitization- Paleoseawater, Karstification-meteoric freshwater and seawater	Early dolomitization- Paleoseawater, Karstification-meteoric fireshwater and seawater	early dolomitization- Paleoseawater	Early dolomitization-Paleoseawater, karstification-meteoric freshwater and seawater	Paleoseawater, Early dolomitization- Paleoseawater, Karstification-meteoric freshwater and seawater
Mesogenetic diagenetic stage Late diagenetic stage	Hydrocarbon charge, ge Hydrothermal fluids (such as organic acids, CO ₂ and H ₂ S) ic	Hydrocarbon charge, Low-temperature hydrothermal fluids Hydrocarbon charge, Tectonic-hydrothermal fluids (such as organic acids, CO ₂ and H ₂ S)	Hydrocarbon charge, hydrocarbon charge, ow-temperature cow-temperature hydrothermal fluids hydrocarbon charge, hydrocarbon charge, hydrocarbon charge, hydrocarbon charge, hydrocarbon charge, hydrocarbon charge, fectonic-hydrothermal fluids Tectonic-hydrothermal fluids anch as organic acids, CO ₂ (such as organic acids, CO ₂ and H ₂ S) and H ₂ S)		Hydrocarbon charge, Hydrocarbon charge, Hydrothermal fluids (such as organic as organic acids, CO ₂ and acids, CO ₂ and H ₂ S)	Hydrocarbon charge, Hydrothermal fluids (such as organic acids, CO ₂ and H ₂ S)
References	Jiang et al. (2018); Jiang et al. (2019); Ma et al. (2019); Qian et al. (2023)	This study	Su et al. (2022); Jiang et al. (2023)	Song et al. (2014); Deng et al. (2018); Wang et al., 2023a,b,c	Shi et al. (2017); Yang et al. (2020); Li et al. (2020); Guo et al. Tang et al. (2022) (2023); Luo et al. (2023)	Li et al. (2020); Guo et a (2023); Luo et al. (2023)

Subsequently, the massive silicification (QZ2) and TSR preserved the reservoir porosity to certain extent during the Hercynian to Indochinese orogenic period.

(3) The coupled effects of paleofluid evolution on ultra-deep microbialite reservoir modification such as reservoir spaces being produced from the basin-scale karstification in the epigenetic diagenetic stage, enlarged during hydrocarbon migration in the mesogenetic diagenesis and preserved to a certain extent into the late diagenetic processes, which would provide a reference for further ultra-deep Precambrian microbiallite hydrocarbon exploration worldwide.

CRediT authorship contribution statement

Xin Jin: Writing — original draft, Investigation. Jin-Min Song: Writing — review & editing, Supervision, Project administration, Funding acquisition. Shu-Gen Liu: Validation, Resources, Project administration. Bin Wang: Writing — review & editing. Di Yang: Resources, Data curation. Zhi-Wu Li: Investigation, Data curation. Li-Zhou Tian: Data curation, Conceptualization. Hao-Shuang Deng: Visualization, Investigation, Data curation. Shan Ren: Investigation. Jia-Min Xue: Investigation. Jia-Xin Guo: Investigation. Zhao-Yi Zhang: Investigation. Xing-Peng Shao: Investigation.

Declaration of competing interest

The authors declare that they have no known competing financial interests or personal relationships that could have appeared to influence the work reported in this paper.

Acknowledgements

This study was jointly supported by the National Natural Science Foundation of China (Nos. 41872150, 42230310) and the Joint Funds of National Natural Science Foundation of China (Grant No. U19B6003). We would like to give thanks to the editors and anonymous reviewers for their suggestions on the manuscript improvement.

Appendix A. Supplementary data

Supplementary data to this article can be found online at https://doi.org/10.1016/j.petsci.2024.10.001.

References

Bau, M., Dulski, P., 1996. Distribution of yttrium and rare-earth elements in the penge and kuruman iron-formations, transvaal supergroup, South Africa. Precambrian Res. 79 (1–2), 37–55. https://doi.org/10.1016/0301-9268(95) 00087-9

Bodnar, R.J., 1993. Revised equation and table for determining the freezing point depression of H_2O -NaCl solutions. Geochim. Cosmochim. Acta 57 (3), 683-684. https://doi.org/10.1016/0016-7037(93)90378-A.

Bourdet, J., Pironon, J., Levresse, G., 2010. Petroleum accumulation and leakage in a deeply buried carbonate reservoir, Níspero field (Mexico). Mar. Petrol. Geol. 27 (1), 126–142. https://doi.org/10.1016/j.marpetgeo.2009.07.003.

Burns, S.J., Haudenschild, U., Matter, A., 1994. The strontium isotopic composition of carbonates from the late Precambrian (~ 560-540 Ma) Huqf Group of Oman. Chem. Geol. 111 (1-4), 269-282. https://doi.org/10.1016/0009-2541(94) 90094-9.

Cai, C.F., He, W.X., Jiang, L., Li, K.K., Xiang, L., Jia, L.Q., 2014. Petrological and geochemical constraints on porosity difference between Lower Triassic sourand sweet-gas carbonate reservoirs in the Sichuan Basin. Mar. Petrol. Geol. 56, 34–50. https://doi.org/10.1016/j.marpetgeo.2014.04.003.

Cai, C.F., Hu, W.S., Worden, R.H., 2001. Thermochemical sulphate reduction in Cambro—Ordovician carbonates in central Tarim. Mar. Petrol. Geol. 18, 729—741. https://doi.org/10.1016/S0264-8172(01)00028-9.

Cai, C.F., Worden, R.H., Bottrell, S.H., Wang, L., Yang, C., 2003. Thermochemical

sulphate reduction and the generation of hydrogen sulphide and thiols (mercaptans) in Triassic carbonate reservoirs from the Sichuan Basin, China. Chem. Geol. 202 (1–2), 39–57. https://doi.org/10.1016/S0009-2541(03)00209-2.

- Cai, C.F., Xie, Z.Y., Worden, R.H., Hu, G.Y., Wang, L.S., He, H., 2004. Methane-dominated thermochemical sulphate reduction in the Triassic feixianguan formation east Sichuan Basin, China: towards prediction of fatal H₂S concentrations. Mar. Petrol. Geol. 21 (10), 1265–1279. https://doi.org/10.1016/j.marpetgeo.2004.09.003.
- Conliffe, J., Azmy, K., Greene, M., 2012. Dolomitization of the lower Ordovician Catoche formation: implications for hydrocarbon exploration in western Newfoundland. Mar. Petrol. Geol. 30 (1), 161–173. https://doi.org/10.1016/ i.marpetgeo.2011.10.007.
- Cruz, N.M., Cruz, J.M., Teixeira, L.M., da Costa, M.M., de Oliveira, L.B., Urasaki, E.N., Bispo, T.P., de Sá Jardim, M., Grochau, M.H., Maul, A., 2021. Tupi Nodes pilot: a successful 4D seismic case for Brazilian presalt reservoirs. Lead. Edge 40 (12), 886–896. https://doi.org/10.1190/tle40120886.1.
- Da Cruz, C.A., Severiano Ribeiro, H.J.P., da Silva, E.B., 2021. Exploratory plays of the Foz do Amazonas Basin, NW portion, in deep and ultra-deep waters, Brazilian Equatorial Margin. J. South Am. Earth Sci. 111, 103475. https://doi.org/10.1016/i.isames.2021.103475.
- Dai, J.X., Ni, Y.Y., Qin, S.F., Huang, S.P., Peng, W.L., Han, W.X., 2018. Geochemical characteristics of ultra-deep natural gas in the Sichuan Basin, SW China. Petrol. Explor. Dev. 45 (4), 619–628. https://doi.org/10.1016/S1876-3804(18)30067-3.
- Deng, S.B., Guan, P., Pang, L., Liu, P.X., Jin, Y.Q., Zhang, Y.Q., 2018. Genesis of excellent Xiaoerbulak microbial carbonate reservoir in Kalpin area of Tarim Basin, NW China. Acta Sedimentol. Sin. 36, 1218–1232. https://doi.org/10.14027/j.issn.1000-0550.2018.084 (in Chinese).
- Ding, Y., Chen, D.Z., Zhou, X.Q., Guo, C., Huang, T.Y., Zhang, G.J., 2019. Cavity-filling dolomite speleothems and submarine cements in the Ediacaran Dengying microbialites, South China: responses to high-frequency sea-level fluctuations in an 'aragonite-dolomite sea'. Sedimentology 66, 2511–2537. https://doi.org/ 10.1111/sed.12605.
- Ehrenberg, S.N., Nadeau, P.H., Steen, ø., 2009. Petroleum reservoir porosity versus depth: influence of geological age. AAPG Bull. 93 (10), 1281–1296. https://doi.org/10.1306/06120908163.
- Fainstein, R., Krueger, A., Ueipass Mohriak, W., 2019. Ultra-deepwater seismic plays offshore Brazil — future drilling off Santos and Campos basins. Interpretation 7 (4), SH99—SH109. https://doi.org/10.1190/INT-2018-0251.1.
- Fan, J.J., Jian, H., Lu, X.S., Liu, Q., Liu, S.B., Ma, X.Z., Huang, S.P., Zeng, F.Y., Tian, H., Xie, W.R., 2022. Pressure evolution and hydrocarbon accumulation process of Sinian Dengying Fornation gas reservoirs in the Penglai area, Sichuan Basin. Nat. Gas. Ind. 42 (12), 32–43. https://doi.org/10.3787/j.issn.1000-0976.2022.12.004 (in Chinese).
- Feng, M.Y., Wu, P.C., Qiang, Z.T., Liu, X.H., Duan, Y., Xia, M.L., 2017. Hydrothermal dolomite reservoir in the Precambrian Dengying Formation of central Sichuan basin, Southwestern China. Mar. Petrol. Geol. 82, 206–219. https://doi.org/10.1016/j.marpetgeo.2017.02.008.
- Guo, R.J., Ji, Y.L., Ma, Z.T., Wan, H.F., Yang, D.J., Ji, H.C., Bao, Z.D., Zhou, Y., Fang, C., Lu, K., Liu, J.X., 2023. Mechanism and development model of karst reservoir in the Wumishan Formation in xiong'an new area. J. Palaeogeogr. 25 (1), 180–197. https://doi.org/10.7605/gdlxb.2023.01.012 (in Chinese).
- Han, C.C., Lin, C.Y., Lu, X.B., Tian, J.J., Ren, L.H., Ma, C.F., 2019. Petrological and geochemical constraints on fluid types and formation mechanisms of the Ordovician carbonate reservoirs in Tahe Oilfield, Tarim Basin, NW China. J. Pet. Sci. Eng. 178, 106–120. https://doi.org/10.1016/j.petrol.2019.03.010.
- He, Z.L., Ma, Y.S., Zhu, D.Y., Duan, T.Z., Geng, J.H., Zhang, J.T., Ding, Q., Qian, Y.X., Wo, Y.J., Gao, Z.Q., 2021. Theoretical and technological progress and research direction of deep and ultra-deep carbonate reservoirs. Oil Gas Geol. 42 (3), 533–546. https://doi.org/10.11743/ogg20210301 (in Chinese).
- He, Z.L., Zhang, J.T., Ding, Q., You, D.H., Peng, S.T., Zhu, D.Y., Qian, Y.X., 2017. Factors controlling the formation of high-quality deep to ultra-deep carbonate reservoirs. Oil Gas Geol. 38 (4), 633–644. https://doi.org/10.11743/ogg20170401 and 763 (in Chinese).
- Hu, Y.J., Cai, C.F., Liu, D.W., Pederson, C.L., Jiang, L., Shen, A.J., Immenhauser, A., 2020a. Formation, diagenesis and palaeoenvironmental significance of upper Ediacaran fibrous dolomite cements. Sedimentology 67, 1161–1187. https://doi.org/10.1111/sed.12683.
- Hu, Y.J., Cai, C.F., Li, Y., Liu, D.W., Wei, T.Y., Wang, D.W., Jiang, L., Ma, R.T., Shi, S.Y., Immenhauser, A., 2023. Sedimentary and diagenetic archive of a deeply-buried, upper Ediacaran microbialite reservoir, S.W. China. AAPG Bull. 107 (3), 387–412. https://doi.org/10.1306/08232221122.
- Hu, Y.J., Cai, C.F., Pederson, C.L., Liu, D.W., Jiang, L., He, X.Y., Shi, S.Y., Immenhauser, A., 2020b. Dolomitization history and porosity evolution of a giant, deeply buried Ediacaran gas field (Sichuan Basin, China). Precambrian Res. 338, 105595. https://doi.org/10.1016/j.precamres.2020.105595.
- Huang, Y.H., He, S., Guo, X.W., Wu, Z.R., Zhai, G.Y., Huang, Z.Q., Zhang, M., Xiao, Q.L., 2021. Pressure—temperature—time—composition (P—T—t—x) of paleo—fluid in Permian organic—rich shale of Lower Yangtze Platform, China: insights from fluid inclusions in fracture cements. Mar. Petrol. Geol. 126, 104936. https://doi.org/10.1016/j.marpetgeo.2021.104936.
- James, C., Karemazmy, L., Knight, D., Lavoie, 2009. Dolomitization of the lower Ordovician watts bight formation of the st. George group, western Newfoundland: evidence of hydrothermal fluid alteration. Can. J. Earth Sci. 46 (4), 247–261. https://doi.org/10.1139/E09-019.
- Jiang, G.Q., Kaufman, A.J., Christie-Blick, N., Zhang, S.H., Wu, H.C., 2007. Carbon

isotope variability across the Ediacaran Yangtze platform in South China: implications for a large surface-to-deep ocean δ^{13} C gradient. Earth Planet Sci. Lett. 261 (1–2), 303–320. https://doi.org/10.1016/j.epsl.2007.07.009.

- Jiang, L., Hu, A.P., Ou, Y.L., Liu, D.W., Hu, Y.J., Tang, Y.J., Sun, P., Liu, Y.Y., Wang, Z.C., Cai, C.F., 2023. Diagenetic evolution and effects on reservoir development of the dengying and longwangmiao formations, Central Sichuan Basin, Southwestern China. Petrol. Sci. 20 (6), 3379–3393. https://doi.org/10.1016/j.petsci.2023.09.025.
- Jiang, L., Hu, S.Y., Zhao, W.Z., Xu, Z.H., Shi, S.Y., Fu, Q.L., Zeng, H.L., Liu, W., Fall, A., 2018a. Diagenesis and its impact on a microbially derived carbonate reservoir from the middle Triassic Leikoupo formation, Sichuan Basin, China. AAPG Bull. 102 (12), 2599–2628. https://doi.org/10.1306/05111817021.
- Jiang, L., Worden, R.H., Yang, C.B., 2018b. Thermochemical sulphate reduction can improve carbonate petroleum reservoir quality. Geochim. Cosmochim. Acta 223, 127–140. https://doi.org/10.1016/j.gca.2017.11.032.
 Jiang, L., Xu, Z.H., Shi, S.Y., Liu, W., 2019. Multiphase dolomitization of a
- Jiang, L., Xu, Z.H., Shi, S.Y., Liu, W., 2019. Multiphase dolomitization of a microbialite-dominated gas reservoir, the middle Triassic Leikoupo formation, Sichuan Basin, China. J. Petrol. Sci. Eng. 180, 820–834. https://doi.org/10.1016/ i.petrol.2019.05.014.
- Jiang, Y.Q., Tao, Y.Z., Gu, Y.F., Wang, J.B., Qiang, Z.T., Jiang, N., Lin, G., Jiang, C., 2016. Hydrothermal dolomitization in Sinian Dengying Formation, Gaoshiti-Moxi area, Sichuan Basin, SW China. Petrol. Explor. Dev. 43 (1), 51–60. https://doi.org/10.1016/S1876-3804(16)30006-4.
- Kolchugin, A., Immenhauser, A., Morozov, V., Walter, B., Eskin, A., Korolev, E., Neuser, R., 2020. A comparative study of two Mississippian dolostone reservoirs in the Volga-Ural Basin, Russia. J. Asian Earth Sci. 199, 104465. https://doi.org/ 10.1016/j.jseaes.2020.104465.
- Kulaksız, S., Bau, M., 2007. Contrasting behaviour of anthropogenic gadolinium and natural rare earth elements in estuaries and the gadolinium input into the North Sea. Earth Planet Sci. Lett. 260 (1–2), 361–371. https://doi.org/10.1016/ j.epsl.2007.06.016.
- Li, C.W., Liu, K.Y., Liu, J.L., 2023. A petroliferous Ediacaran microbial-dominated carbonate reservoir play in the central Sichuan Basin, China: characteristics and diagenetic evolution. Precambrian Res. 384, 106937. https://doi.org/ 10.1016/j.precamres.2022.106937.
- Li, P.W., He, Z.L., Luo, P., Jin, T.F., Zhang, Y., Feng, J.B., Song, J.M., Xu, S.L., 2020. Characteristics of and main factors controlling dolomite reservoir of Gaoyuzhuang-Wumishan Formations in the Jixian System, the north of North China. Oil Gas Geol. 41 (1), 26–36. https://doi.org/10.11743/ogg20200103 (in Chinese).
- Li, W., Liu, J.J., Deng, S.H., Zhang, B.M., Zhou, H., 2015. The nature and role of Late Sinian-Early Cambrian tectonic movement in Sichuan Basin and its adjacent areas. Acta Petrol. Sin. 36, 546–556. https://doi.org/10.7623/syxb201505003, 563 (in Chinese).
- Li, W., Yi, H.Y., Hu, W.S., Yang, G., Xiong, X., 2014. Tectonic evolution of Caledonian paleohigh in the Sichuan Basin and its relationship with hydrocarbon accumulation. Nat. Gas. Ind. B 1 (1), 8–15. https://doi.org/10.1016/j.ngib.2014.10.007.
- Li, Y.S., Liu, G.D., Song, Z.Z., Sun, M.L., Tian, X.W., Yang, D.L., Zhu, L.Q., 2024. Crude oil cracking under geological conditions: a case study of the Ediacaran reservoir, central Sichuan Basin, China. Fuel 364, 131063. https://doi.org/10.1016/j.fuel.2024.131063.
- Liu, Q.Y., Zhu, D.Y., Jin, Z.J., Liu, C.Y., Zhang, D.W., He, Z.L., 2016a. Coupled alteration of hydrothermal fluids and thermal sulfate reduction (TSR) in ancient dolomite reservoirs – an example from Sinian Dengying Formation in Sichuan Basin, southern China. Precambrian Res. 285, 39–57. https://doi.org/10.1016/ j.precamres.2016.09.006.
- Liu, S.G., Song, J.M., Luo, P., Qing, H.R., Lin, T., Sun, W., Li, Z.W., Wang, H., Peng, H.L., Yu, Y.Q., Long, Y., Wan, Y.B., 2016b. Characteristics of microbial carbonate reservoir and its hydrocarbon exploring outlook in the Sichuan Basin, China. J. Chengdu Univ. Technol. (Sci. Technol. Ed.) 43 (129–152), 1671–9727. https://doi.org/10.3969/j.issn.1671-9727.2016.02.01 (in Chinese).
- Liu, S.G., Song, J.M., Zhao, Y.H., Zhong, Y., Song, L.K., Tian, Y.H., Liang, F., Yin, K.W., Li, J.L., 2014. Controlling factors of formation and distribution of Lower Cambrian Longwangmiao Formation high-quality reservoirs in Sichuan basin. J. Chengdu Univ. Technol. (Sci. Technol. Ed.) 41, 657–670. https://doi.org/ 10.3969/j.issn.1671-9727.2014.06.01 (in Chinese).
- Liu, S.G., Sun, W., Luo, Z.L., Song, J.M., Zhong, Y., Tian, Y.H., Peng, H.L., 2013. Xingkai taphrogenesis and petroleum exploration from upper sinian to cambrian strata in Sichuan Basin, China. J. Chengdu Univ. Technol. (Sci. Technol. Ed.) 40, 511–520. https://doi.org/10.3969/j.issn.1671-9727.2013.05.03 (in Chinese).
- Liu, S.G., Yang, Y., Deng, B., Zhong, Y., Wen, L., Sun, W., Li, Z.W., Jansa, L., Li, J.X., Song, J.M., Zhang, X.H., Peng, H.L., 2021. Tectonic evolution of the Sichuan Basin, southwest China. Earth Sci. Rev. 213, 103470. https://doi.org/10.1016/ j.earscirev.2020.103470.
- Luo, N., Xue, H., Li, J.M., Zhang, J., Zhu, P., Tang, X.Q., Han, C.Y., Ye, D.S., 2023. Characteristics and evolution of microbial dolomite reservoir of Wumishan Formation in Renqiu buried hill, Jizhong Depression. Marine Origin Petroleum Geology 28, 144—156. https://doi.org/10.3969/j.issn.1672-9854.2023.02.004 (in Chinese).
- Ma, K., Wen, L., Zhang, B.J., Li, Y., Zhong, J.Y., Wang, Y.L., Peng, H.L., Zhang, X.H., Yan, W., Ding, Y., Chen, X., 2022. Segmented evolution of Deyang-Anyue erosion rift trough in Sichuan Basin and its significance for oil and gas exploration, SW China. Petrol. Explor. Dev. 49 (2), 313–326. https://doi.org/10.1016/S1876-3804(22)60026-0
- Ma, Y.S., Cai, X.Y., Li, H.L., Zhu, D.Y., Zhang, J.T., Yang, M., Duan, J.B., Deng, S.,

You, D.H., Wu, C.Y., Chen, S.R., 2023. New insights into the formation mechanism of deep-ultra-deep carbonate reservoirs and the direction of oil and gas exploration in extra-deep strata. Earth Sci. Front. 30 (6), 1–13. https://doi.org/10.13745/j.esf.sf.2023.2.35 (in Chinese).

- Ma, Y.S., He, Z.L., Zhao, P.R., Zhu, H.Q., Han, J., You, D.H., Zhang, J.T., 2019. A new progress in formation mechanism of deep and ultra-deep carbonate reservoir. Acta Petrol. Sin. 40, 1415–1425. https://doi.org/10.7623/syxb201912001 (in Chinese).
- McLennan, S.M., 1989. Rare earth elements in sedimentary rocks; influence of provenance and sedimentary processes. Rev. Mineral. Geochem. 21 (1), 169–200. https://doi.org/10.1515/9781501509032-010.
- Meng, F.W., Ni, P., Schiffbauer, J.D., Yuan, X.L., Zhou, C.M., Wang, Y.G., Xia, M.L., 2011. Ediacaran seawater temperature: evidence from inclusions of Sinian halite. Precambrian Res. 184, 63–69. https://doi.org/10.1016/j.precamres.2010.10.004.
- Meng, W., Niu, Z.C., Jiang, Y., Hao, X.F., Yang, Y.H., Jiang, S., Li, J.Y., An, T.X., Fang, L., Ren, X.Y., Cheng, R., 2024. Evolution processes and diagenetic response of paleopore fluids in continental rift basin: a case study of Bonan Sag. Energy Sci. Eng. 233, 212547. https://doi.org/10.1016/j.geoen.2023.212547.
- 233, 212547. https://doi.org/10.1016/j.geoen.2023.212547.
 Ni, Z.Y., Chen, Z.H., Li, M.J., Yang, C.Y., Wen, L., Hong, H.T., Luo, B., 2020. Trace element characterization of bitumen constraints on the hydrocarbon source of the giant gas field in Sichuan Basin, South China. Geol. J. 55 (1), 317–329. https://doi.org/10.1002/gij.3412.
- Paula-Santos, G.M., Caetano-Filho, S., Enzweiler, J., Navarro, M.S., Babinski, M., Guacaneme, C., Kuchenbecker, M., Reis, H., Trindade, R.I.F., 2020. Rare earth elements in the terminal Ediacaran Bambuí Group carbonate rocks (Brazil): evidence for high seawater alkalinity during rise of early animals. Precambrian Res. 336, 105506. https://doi.org/10.1016/j.precamres.2019.105506.
- Petrash, D.A., Bialik, O.M., Bontognali, T.R.R., Vasconcelos, C., Roberts, J.A., McKenzie, J.A., Konhauser, K.O., 2017. Microbially catalyzed dolomite formation: from near-surface to burial. Earth Sci. Rev. 171, 558–582. https://doi.org/10.1016/j.earscirev.2017.06.015.
- Qian, Y.X., Wu, H.Z., Zhou, L.F., Dong, S.F., Wang, Q.X., Song, X.B., Deng, M.Z., Li, Y., 2023. Diagenesis and porosity evolution of microbial carbonate rocks undergone a deep burial history:Taking the Leikoupo Formation of Middle Triassic in western Sichuan Basin as an example. Oil Gas Geol. 44 (1), 55–74. https://doi.org/10.11743/ogg20230105 (in Chinese).
- Sánchez-Román, M., McKenzie, J.A., Wagener, A.d.L.R., Rivadeneyra, M.A., Vasconcelos, C., 2009. Presence of sulfate does not inhibit low-temperature dolomite precipitation. Earth Planet Sci. Lett. 285 (1–2), 131–139. https://doi.org/10.1016/j.epsl.2009.06.003.
- Scotese, C., 2009. Late Proterozoic plate tectonics and palaeogeography: a tale of two supercontinents, Rodinia and Pannotia. Geol. Soc. Spec. Publ. 326, 67–83. https://doi.org/10.1144/SP326.4.
- Shen, A.J., Hu, A.P., Cheng, T., Liang, F., Pan, W.Q., Feng, Y.X., Zhao, J.X., 2019. Laser ablation in situ U-Pb dating and its application to diagenesis-porosity evolution of carbonate reservoirs. Petrol. Explor. Dev. 46 (6), 1127–1140. https://doi.org/10.1016/S1876-3804(19)60268-5.
- Shen, A.J., Zhao, W.Z., Hu, A.P., Wang, H., Liang, F., Wang, Y.S., 2021. The dating and temperature measurement technologies for carbonate minerals and their application in hydrocarbon accumulation research in the paleo-uplift in central Sichuan Basin, SW China. Petrol. Explor. Dev. 48 (3), 476–487. https://doi.org/ 10.1016/S1876-3804(21)60045-9.
- Shi, S.Y., Liu, W., Huang, Q.Y., Wang, T.S., Zhou, H., Wang, K., Ma, K., 2017. Dolostone reservoir characteristic and its formation mechanism in Qigebulake formtion, Sinian, north Tarim Basin. Nat. Gas Geosci. 28 (8), 1226—1234. https://doi.org/10.11764/j.issn.1672-1926.2016.11.006 (in Chinese).
- Song, J.M., Luo, P., Yang, S.S., Yang, D., Zhou, C.M., Li, P.W., Zhai, X.F., 2014. Reservoirs of lower cambrian microbial carbonates, Tarim Basin, NW China. Petrol. Explor. Dev. 41 (4), 449–459. https://doi.org/10.1016/S1876-3804(14)60051-3.
- Song, J.M., Liu, S.G., Li, Z.W., Luo, P., Yang, D., Sun, W., Peng, H.L., Yu, Y.Q., 2017. Characteristics and controlling factors of microbial carbonate reservoirs in the upper sinian Dengying Formation in the Sichuan Basin, China. Oil Gas Geol. 38 (4), 741–752. https://doi.org/10.11743/ogg20170411 (in Chinese).
- Song, J.M., Liu, S.G., Qing, H.R., Jansa, L., Li, Z.W., Luo, P., Yang, D., Sun, W., Peng, H.L., Lin, T., 2018. The depositional evolution, reservoir characteristics, and controlling factors of microbial carbonates of Dengying Formation in upper Neoprotozoic, Sichuan Basin, Southwest China. Energy Explor. 36 (4), 591–619. https://doi.org/10.1177/01445987177439.
- Su, A., Chen, H.H., Feng, Y.X., Zhao, J.X., Wang, Z.C., Hu, M.Y., Jiang, H., Nguyen, A.D., 2022. In situ U-Pb dating and geochemical characterization of multi-stage dolomite cementation in the Ediacaran Dengying Formation, Central Sichuan Basin, China: constraints on diagenetic, hydrothermal and paleo-oil filling events. Precambrian Res. 368, 106481. https://doi.org/10.1016/jing.ccampes.2021.106481
- Su, J., Wang, X.M., Yang, H.J., Yu, F., Li, Y., Ma, S.H., Wei, C.Y., Weng, N., Yang, Y.P., 2021. Hydrothermal alteration and hydrocarbon accumulations in ultra-deep carbonate reservoirs along a strike-slip fault system, Tarim Basin, NW China. J. Pet. Sci. Eng. 203, 108605. https://doi.org/10.1016/j.petrol.2021.108605.
- Sun, T.J., Luo, X.P., Mi, W.T., Woods, A., Chiarella, D., Qing, H.R., Ma, Y.S., Kou, X.L., Shen, Z.M., Xu, G.S., Yuan, H.F., Liang, J.J., Xu, F.H., Wang, H., Gong, X.X., Luo, J., Jin, T.F., Lv, X.W., 2023. Characterization of ultra-deeply buried middle Triassic Leikoupo marine carbonate petroleum system (!) in the Western Sichuan depression, China. Mar. Petrol. Geol. 150, 106099. https://doi.org/10.1016/j.marpetgeo.2023.106099.
- Tahata, M., Ueno, Y., Ishikawa, T., Sawaki, Y., Murakami, K., Han, J., Shu, D., Li, Y.,

Guo, J., Yoshida, N., 2013. Carbon and oxygen isotope chemostratigraphies of the Yangtze platform, South China: decoding temperature and environmental changes through the Ediacaran. Gondwana Res. 23 (1), 333–353. https://doi.org/10.1016/j.gr.2012.04.005.

- Tang, J.G., Hu, W.S., Li, W., Zhang, G.Y., 2013. Prediction of weathering paleokarst reservoirs by combining paleokarst landform with unconformity: a case study of Sinian Dengying Formation in Leshan-Longnusi paleo-uplift, Sichuan Basin. Petrol. Explor. Dev. 40 (6), 722–730. https://doi.org/10.1016/S1876-3804(13)
- Tang, P., Chen, D.Z., Wang, Y.Z., Ding, Y., El-Shafeiy, M., Yang, B., 2022. Diagenesis of microbialite-dominated carbonates in the upper ediacaran Qigebrak Formation, NW Tarim Basin, China: implications for reservoir development. Mar. Petrol. Geol. 136, 105476. https://doi.org/10.1016/j.marpetgeo.2021.105476.
- Wang, G.W., Hao, F., Zou, H.Y., Li, P.P., 2023a. Causes of variation in the concentration and distribution of H₂S in carbonate reservoirs of the Feixianguan Formation, lower triassic in the eastern Sichuan Basin. Energy Sci. Eng. 221, 211381. https:// doi.org/10.1016/j.geoen.2022.211381.
- Wang, H., Liu, S.G., Hou, M.C., Zhang, B.J., Song, J.M., Zhao, R.R., Ding, Y., Han, Y.Y., Li, Z.W., 2022. Petrological and micrometer-scale geochemical constraints on chert origins in the Dengying Formation, Yangtze Block, South China: implications for Late Ediacaran hydrothermal activity and tectonic setting. Precambrian Res. 370, 106531. https://doi.org/10.1016/ji.precamres.2021.106531.
- Wang, P., Wang, G.W., Chen, Y.Q., Hao, F., Yang, X.Z., Hu, F.J., Zhou, L., Yi, Y., Yang, G., Wang, X.X., Cong, F.Y., 2023b. Formation and preservation of ultra-deep high-quality dolomite reservoirs under the coupling of sedimentation and diagenesis in the central Tarim Basin, NW China. Mar. Petrol. Geol. 149, 106084. https://doi.org/10.1016/j.marpetgeo.2022.106084.
- Wang, Z.Y., Ning, K.K., Qu, H.Z., Hu, A.P., Zhang, Y.F., Chen, W., Luo, X.S., Zhang, X.Y., 2023c. Pore characteristics, origin, and evolution of different dolomites in the Cambrian Xiaoerbulak Formation in the aksu area. Acta Sedimentol. Sin. 41 (1), 256–269. https://doi.org/10.14027/j.issn.1000-0550.2021.157 (in Chinese).
- Wei, G.Q., Yang, W., Xie, W.R., Su, N., Xie, Z.Y., Zeng, F.Y., Ma, S.Y., Jin, H., Wang, Z.H., Zhu, Q.Y., Hao, C.G., Wang, X.D., 2022. Formation mechanisms, potentials and exploration practices of large lithologic gas reservoirs in and around an intra-cratonic rift: taking the Sinian—Cambrian of Sichuan Basin as an example. Petrol. Explor. Dev. 49 (3), 530–545. https://doi.org/10.1016/S1876-3804(22) 60044-2
- Xu, Z.H., Lan, C.J., Zhang, B.J., Hao, F., Lu, C.J., Tian, X.W., Zou, H.Y., 2022. Impact of diagenesis on the microbial reservoirs of the terminal ediacaran Dengying Formation from the central to northern Sichuan Basin, SW China. Mar. Petrol. Geol. 146, 105924. https://doi.org/10.1016/j.marpetgeo.2022.105924.
- Yan, R.J., Xu, G.S., Xu, F.H., Song, J.M., Yuan, H.F., Luo, X.P., Fu, X.D., Cao, Z.Y., 2022. The multistage dissolution characteristics and their influence on mound—shoal complex reservoirs from the Sinian Dengying Formation, southeastern Sichuan Basin, China. Mar. Petrol. Geol. 139, 105596. https://doi.org/10.1016/ j.marpetgeo.2022.105596.
- Yang, H.X., Hu, A.P., Zheng, J.F., Liang, F., Luo, X.Y., Feng, Y.X., Shen, A.J., 2020. Application of mapping and dating techniques in the study of ancient carbonate reservoirs: a case study of Sinian Qigebrak Formation in northwestern Tarim Basin, NW China. Petrol. Explor. Dev. 47 (5), 1001–1013. https://doi.org/10.1016/ S1876-3804(20)60112-4.
- Yang, Y., Wen, L., Song, Z.Z., Zhang, B.J., Yan, W., Zhou, G., Tian, X.W., Zhong, Y., He, Y., Ma, K., Li, K.Y., Yang, D.L., Sun, Y.T., Ge, B.F., Yang, Z.Z., 2022. Breakthrough and potential of natural gas exploration in multi-layer system of Penglai gas area in the north of central Sichuan paleo-uplift. Acta Petrol. Sin. 43 (10), 1351–1368+1394. https://doi.org/10.7623/syxb202210001 (in Chinese).
- Yu, Q., Mu, C.L., Zhang, H.Q., Tan, Q.Y., Xu, X.S., Yan, J.F., 2011. Sedimentary evolution and reservoir distribution of northern Upper Yangtze plate in Sinian-Early Paleozoic. Acta Petrol. Sin. 27, 672–680 h ttps://doi.org/SUN:YSXB.0.2011-03-008 (in Chinese).
- Zhai, X.F., Luo, P., Gu, Z.D., Jiang, H., Zhang, B.M., Wang, Z.C., Wang, T.S., Wu, S.T., 2020. Microbial mineralization of botryoidal laminations in the upper Ediacaran dolostones, western Yangtze platform, SW China. J. Asian Earth Sci. 195, 104334. https://doi.org/10.1016/j.jseaes.2020.104334.
- Zhang, P.W., Liu, G.D., Cai, C.F., Li, M.J., Chen, R.Q., Gao, P., Xu, C.L., Wan, W.C., Zhang, Y.Y., Jiang, M.Y., 2019. Alteration of solid bitumen by hydrothermal heating and thermochemical sulfate reduction in the Ediacaran and Cambrian dolomite reservoirs in the Central Sichuan Basin, SW China. Precambrian Res. 321, 277–302. https://doi.org/10.1016/j.precamres.2018.12.014.
- Zhao, D.F., Hu, G., Wang, L.C., Li, F., Tan, X.C., She, M., Zhang, W.J., Qiao, Z.F., Wang, X.F., 2020. RETRACTED: sedimentary characteristics and origin of dolomitic ooids of the terminal Edicaran Dengying Formation at Yulin (Chongqing, South China). Palaeogeogr. Palaeoclimatol. Palaeoecol. 544, 109601. https://doi.org/10.1016/j.palaeo.2020.109601.
- Zhao, D.F., Tan, X.C., Hu, G., Wang, L.C., Wang, X.F., Qiao, Z.F., Luo, S.C., Tang, H., 2021. Characteristics and primary mineralogy of fibrous marine dolomite cements in the end-Ediacaran Dengying Formation, South China: implications for aragonite—dolomite seas. Palaeogeogr. Palaeoclimatol. Palaeoecol. 581, 110635. https://doi.org/10.1016/j.palaeo.2021.110635.
- Zhao, G.C., Wang, Y.J., Huang, B.C., Dong, Y.P., Li, S.Z., Zhang, G.W., Yu, S., 2018. Geological reconstructions of the East Asian blocks: from the breakup of Rodinia to the assembly of Pangea. Earth Sci. Rev. 186, 262–286. https://doi.org/ 10.1016/j.earscirev.2018.10.003.
- Zhao, W.Z., Shen, A.J., Hu, S.Y., Zhang, B.M., Pan, W.Q., Zhou, J.G., Wang, Z.C., 2012. Geological conditions and distributional features of large-scale carbonate

reservoirs onshore China. Petrol. Explor. Dev. 39 (1), 1-14. https://doi.org/ 10.1016/S1876-3804(12)60010-X.

- Zhao, W.Z., Wang, X.F., Wang, X., Wang, K., Shen, A.J., 2022. Stratigraphic sequence re-determination and lithofacies palaeogeographical characteristics of the sinian Dengying Formation in Sichuan Basin. J. Palaeogeogr. 24, 852–870. https://doi.org/10.7605/gdlxb.2022.05.062 (in Chinese).
- Zhong, Y., Li, Y.L., Zhang, X.B., Liu, S.G., Liu, D.J., Deng, X.J., Chen, S., Sun, W., Chen, Y.H., 2013. Features of extensional structures in pre-Sinian to Cambrian strata, Sichuan Basin, China. J. Chengdu Univ. Technol. (Sci. Technol. Ed.) 40 (5), 498–510. https://doi.org/10.3969/j.issn.1671-9727.2013.05.02 (in Chinese).
- Zhou, H., Li, W., Zhang, B.M., Liu, J.J., Deng, S.H., Zhang, S.B., Shan, X.Q., Zhang, J., Wang, X.B., Jiang, H., 2017. Formation and evolution of intraplatform basin from the late Sinian to early Cambrian in Sichuan Basin, China. Pet. Res. 2 (1), 41–53. https://doi.org/10.1016/j.ptfrs.2017.01.001.
 Zhou, Y., Yang, F.L., Ji, Y.L., Zhou, X.F., Zhang, C.H., 2020. Characteristics and con-
- trolling factors of dolomite karst reservoirs of the Sinian Dengying Formation,

- central Sichuan Basin. Southwestern China. Precambrian Res. 343, 105708. https://doi.org/10.1016/j.precamres.2020.105708
- Zhu, D.Y., Liu, Q.Y., He, Z.L., Ding, Q., Wang, J.B., 2020. Early development and late preservation of porosity linked to presence of hydrocarbons in Precambrian microbialite gas reservoirs within the Sichuan Basin, southern China. Precambrian Res. 342, 105694. https://doi.org/10.1016/j.precamres.2020.105694.
- Zhu, Z.P., Luo, W.J., Pan, R.F., Weng, X.B., Jin, J.N., 2019. The paleogeomorphology restoration of Sinian Deng 4 Member and its control on reservoir formation in the Gaoshiti-Moxi area in central Sichuan Basin. China Petroleum Exploration 24 (6), 730–738. https://doi.org/10.3969/j.issn.1672-7703.2019.06.005 (in Chinese).
- Zou, C.N., Du, J.H., Xu, C.C., Wang, Z.C., Zhang, B.M., Wei, G.Q., Wang, T.S., Yao, G.S., Deng, S.H., Liu, J.J., Zhou, H., Xu, A.A., Yang, Z., Jiang, H., Gu, Z.D., 2014. Formation, distribution, resource potential and discovery of the Sinian-Cambrian giant gas field, Sichuan Basin. SW China. Petrol. Explor. Dev. 41 (3), 278–293. https://doi.org/10.1016/S1876-3804(14)60036-7.